

62 64834

Copy 26
RM SL58F10

SERVICE REPORT

Declassified by authority of NASA
Classification Change Notices No. 167
Dated ** 4/15/69

NACA

RESEARCH MEMORANDUM

for the **DECLASSIFIED- AUTHORITY MEMO U.S. 4508**
U. S. Air Force **RICE TO SHAUKLAS DATED 11/21/68**

**FORWARD HINGE MOMENTS AND LONGITUDINAL STABILITY OF A
1/7-SCALE MODEL OF THE CONVAIR B-58 EXTERNAL STORE
IN A FREE-FLIGHT INVESTIGATION AT MACH
NUMBERS FROM 0.94 TO 2.58**

COORD. NO. AF-204

By James A. Hollinger

Langley Aeronautical Laboratory
Langley Field, Va.

Restriction/Classification Cancelled

(THRU) <i>Mike</i>	(CATEGORY)
(CODE)	
(ACCESSION-NUMBER) <i>37</i>	(NASA CR OR TMX OR AD NUMBER)
(PAGES)	

X 69-71608

FF No. 602(A)

NATIONAL ADVISORY COMMITTEE FOR AERONAUTICS

WASHINGTON

JUN 20 1958

CANARD HINGE MOMENTS AND LONGITUDINAL STABILITY OF A
1/7-SCALE MODEL OF THE CONVAIR B-58 EXTERNAL STORE
IN A FREE-FLIGHT INVESTIGATION AT MACH
NUMBERS FROM 0.94 TO 2.58

COORD. NO. AF-204

By James A. Hollinger

ABSTRACT

Abrupt pitching disturbances were created by step-function movements of the canard surface. Hinge moments of the canard surface were found to be small, a fact which indicated that the hinge line was near the center of pressure. The variation of hinge moment with angle of attack decreased rapidly as Mach number increased from 0.94 to about 1.2 but was more nearly constant at higher Mach numbers. The normal-force-curve slope was found to be smaller than the lift-curve slope predicted by NACA Research Memorandum SL55G22a. The model was statically and dynamically stable.

INDEX HEADINGS

Stores - Airplane Components	1.7.1.1.5
Stability, Longitudinal - Static	1.8.1.1.1
Stability, Longitudinal - Dynamic	1.8.1.2.1
Control, Hinge Moments	1.8.2.5

NACA RM SL58F10

CONFIDENTIAL

CANARD HINGE MOMENTS AND LONGITUDINAL STABILITY OF A
1/7-SCALE MODEL OF THE CONVAIR B-58 EXTERNAL STORE
IN A FREE-FLIGHT INVESTIGATION AT MACH
NUMBERS FROM 0.94 TO 2.58

COORD. NO. AF-204

James A. Hollinger
James A. Hollinger

Approved:

Joseph A. Shortal
Joseph A. Shortal
Chief of Pilotless Aircraft Research Division
Langley Aeronautical Laboratory

rh
(6/2/58)

CONFIDENTIAL

NATIONAL ADVISORY COMMITTEE FOR AERONAUTICS

RESEARCH MEMORANDUM

for the

U. S. Air Force

CANARD HINGE MOMENTS AND LONGITUDINAL STABILITY OF A
1/7-SCALE MODEL OF THE CONVAIR B-58 EXTERNAL STORE
IN A FREE-FLIGHT INVESTIGATION AT MACH
NUMBERS FROM 0.94 TO 2.58

COORD. NO. AF-204

By James A. Hollinger


SUMMARY

A longitudinal stability and control investigation was made over a Mach number range from 0.94 to 2.58 of a 1/7-scale model of the Convair B-58 external store. Normal force, chord force, and static and dynamic stability derivatives formed an important part of the results. Abrupt pitching disturbances were created by step-function movements of the canard surface.

Hinge moments of the canard surface were found to be small, a fact which indicated that the hinge line was near the center of pressure. The variation of hinge moment with angle of attack decreased rapidly as Mach number increased from 0.94 to about 1.2 but was more nearly constant at higher Mach numbers. The normal-force-curve slope was found to be smaller than the lift-curve slope predicted by NACA Research Memorandum SL55G22a. For a center of gravity 2.874 feet behind the nose, the model was statically and dynamically stable.

INTRODUCTION

At the request of the U. S. Air Force, the Langley Pilotless Aircraft Research Division has undertaken a flight-test program of the



Convair B-58 external store, a rocket-powered disposable bomb to be carried beneath the B-58 fuselage. The drag of the store was reported in reference 1. In order to furnish information on the control hinge moments, longitudinal trim, and stability, a 1/7-scale rocket-boosted model of the store with a pulsed canard was flight tested. The test was conducted at the Langley Pilotless Aircraft Research Station at Wallops Island, Va.

SYMBOLS

b	wing span, ft
\bar{c}	mean aerodynamic chord, ft
H	canard-surface hinge moment, in-lb
I_X	moment of inertia about X-axis, ft-lb-sec ²
I_Y	moment of inertia about Y-axis, ft-lb-sec ²
I_Z	moment of inertia about Z-axis, ft-lb-sec ²
M	Mach number, pitching moment about model center of gravity
p	static pressure, lb/sq in.
P	period of longitudinal motion, sec
q	dynamic pressure, lb/sq ft
R	Reynolds number based on \bar{c}_w
S	plan-form area, sq ft
$t_{0.5}$	time in which longitudinal motion damps to one-half amplitude, sec
V_c	speed of sound, ft/sec
W	weight of model, lb
X	longitudinal body axis through center of gravity
Y	lateral body axis through center of gravity

- Z vertical body axis through center of gravity
- α angle of attack, deg
- δ angle of canard deflection, positive when trailing edge is down, deg
- C_c chord-force coefficient, $\frac{\text{Chord force}}{qS_w}$
- C_h canard-surface hinge-moment coefficient, $\frac{H}{12qS_s \bar{c}_s}$
- C_L lift coefficient, $\frac{\text{Lift}}{qS_w}$
- C_m pitching-moment coefficient, $\frac{\text{Pitching moment}}{qS_w \bar{c}_w}$
- C_N normal-force coefficient, $\frac{\text{Normal force}}{qS_w}$
- C_{h_α} $\frac{dC_h}{d\alpha}$ at constant δ , per deg
- C_{h_δ} $\frac{\Delta C_h}{\Delta \delta}$ at $\alpha = 0^\circ$, per deg
- C_{L_α} lift-curve slope, per deg
- C_{N_α} normal-force-curve slope, per deg
- C_{m_α} pitching-moment-curve slope (static stability derivative), per deg
- $C_{m_q} + C_{m_\dot{\alpha}}$ dynamic longitudinal stability derivative (pitch damping derivative), per radian

Subscripts:

- s exposed canard surface
- w wing (total)

CONFIDENTIAL

MODEL

The general arrangement and the dimensions of the 1/7-scale model of the external store are shown in a three-view drawing in figure 1. Figure 2 is a photograph of the model and booster on the launcher. Pertinent physical characteristics are presented in table I. Tables in reference 1 contain further dimensional data, such as store geometry, strut geometry, and actuator fairings. The forward 38 percent of the body was steel and the rest of the body was aluminum. The canard was steel, the tail fins were aluminum, and the wing was aluminum with steel tips. Actuator fairings were simulated on the wing and on the root of the lower vertical fin.


The canard surface was moved abruptly by the pull of a spring on a lever extending from the hinge shaft. The control was held in each deflected position by latches while the spring was being cocked for the opposite pull by a motor-driven crank. The deflection angles of the canard surface were approximately 0.4° and 6.5° . The model and the control system were designed and constructed by Convair, Division of General Dynamics Corp.

A smoke generator was installed within the model to aid visual tracking.

INSTRUMENTATION

An NACA 12-channel telemeter was installed and simultaneous continuous recordings were made of the following quantities: angle of attack; angle of sideslip; control position; control hinge moment; rolling velocity; total pressure; static pressure; normal, transverse, and longitudinal accelerations near the center of gravity; and normal and transverse accelerations in the nose.

Ground-based instrumentation consisted of a Doppler radar unit for measuring model velocity, a modified SCR-584 radar unit for obtaining the model position in space, and a rollsonde receiver sensitive to the telemeter antenna radiation pattern for an additional measurement of the model rolling velocity. Motion-picture records were made of the flight. Atmospheric conditions and wind velocities over the firing range were obtained from a rawinsonde released immediately after the flight.



PREFLIGHT TESTS

The model, as received from the contractor, required extensive modification to provide a more powerful control system. The calibrated range as finally modified was ± 200 inch-pounds. A sketch of the model showing the body system of axes used in the investigation and the sign convention used for hinge moment and control position is given in figure 3.

The actuating spring in the control system was preloaded before each abrupt movement by a motor-driven crank. The presence of the hinge-moment measuring device in the control system required a certain amount of flexibility in the lever extending from the hinge shaft. The force built up in the spring flexed the hinge-shaft lever, and early ground tests showed that the internal moment masked a large portion of the hinge moment. A simple modification of the control system served to reduce internally produced moment but it was not practical to eliminate it.


A preflight recording was taken of the telemeter signals of control position and hinge moment while the control was pulsing. The time history of 1 cycle of control motion is reproduced in figure 4, in which the applied hinge moment is zero and the variations of control deflection and hinge moment are a function only of internal effects. The illustrated sequence of events was duplicated with each succeeding cycle of motion. The section of the record shown in figure 4 was used as a calibration of the drift of the flight recording of the control position for the case of constant aerodynamic hinge moment.

Since control deflection changed with applied hinge moment, a test was made to determine the amount of control linkage flexibility. A moment was applied to the canard surface and its angle read with an inclinometer. The resulting knowledge of control flexibility was used to find the hinge moments throughout the flight test.

The model was shaken by an electromagnetic shaker but there were no significant modes of vibration.

FLIGHT TEST

The model and booster were launched from a zero-length launcher on a gun carriage. The model was boosted to a Mach number of 2.60 by a Nike booster motor which separated from the model at 3.59 seconds after ignition. The conditions of the flight are presented in figures 5 to 7: Reynolds number plotted against Mach number (fig. 5); time histories of Mach number and dynamic pressure (fig. 6); and time histories of altitude, speed of sound, and static pressure (fig. 7).



The recording of control hinge moment stopped at 4.79 seconds past launching time and the recording of angle of sideslip stopped at 13.09 seconds. The canard surface remained undeflected for a short time after separation of the booster rocket and actuating of a switch, after which time the control was snapped to a deflection of about 6.7° by the preloaded spring. The canard surface moved to a deflection near zero at 12.17 seconds past launching time and thereafter regularly moved between deflections of about 0.4° and about 6.5° at time intervals averaging 0.93 second. The transit time to accomplish the change of deflection averaged 0.018 second. In the time interval between 4.02 and 12.17 seconds past launch, the canard surface did not move appreciably, probably due to a stall of the electric cocking of the spring in the actuating system. Although preflight tests had shown generally poor performance, the control system was used in the flight test to save the time for complete redesign and rebuilding of the mechanism.

The actual control deflection was indicated by the control-position recorder, and the external or internal hinge moments produced no errors in the measurement of deflection. The change of control deflection due to hinge moment was accurately known; therefore, the deviation of the control setting was used as a measurement of hinge moment. Data from this source were available throughout the test, including the earlier interval when the hinge-moment instrument was recording.

ACCURACY

From previous experience with similar instrumentation and by inspection of the data described herein, the accuracies of the basic measured quantities were estimated and are shown in table II. Excluding the effect of dynamic-pressure inaccuracies which had an appreciable effect on all derivatives at low speeds, the values of C_{m_α} were affected greatly by inaccuracies in periods and the values of $C_{m_q} + C_{m_{\dot{\alpha}}}$ were affected greatly by inaccuracies in damping time. The cross plots and lift-curve slopes show an amount of scatter that is unusually great for this type of investigation, a fault attributable to something other than any zero-point shift which may have occurred.

The scatter in normal-force curves and in normal-force-curve slope would arise primarily from the pitch amplitude which is relatively small in comparison with the calibrated range of the instruments. The average oscillation in normal acceleration covered one-tenth the calibrated range of the instrument and a typical one covered much less, since the requirements for recording high-speed data necessitated large accelerations for only one brief instant in the long flight test. The forces on the model

were related to the dynamic-pressure curve in figure 6, which shows the brief duration of high values of q .

RESULTS

Hinge Moments

In order to obtain hinge-moment data from the control-position recording, the spring-cocking effect was first removed. Then, the deflection of the unloaded control was subtracted from the corrected recorded deflection to find the change due to hinge moment, which was related to a certain value of hinge moment. Next, hinge-moment coefficient was computed by the equation

$$C_h = \frac{H}{12qS_s \bar{c}_s}$$

The total hinge-moment coefficient was plotted against angle of attack for the two control deflections and slopes taken. The shaded areas in figure 8 encompass all the slopes found by this method. The value of $C_{h\alpha}$ decreased rapidly as Mach number increased from 0.94 to about 1.2 but was nearly constant at higher Mach numbers. A difference in slope for the two control deflections is evident and may have arisen from the change of deflection or change in the trim angle of attack.

When the proper hinge-moment instrument was recording, its values agreed with values found from actuator flexibility within ± 5 percent. The hinge moments were small, never exceeding 120 inch-pounds, and this fact would indicate that the hinge line (53 percent \bar{c}_s) was near the center of pressure.

The faired value of hinge-moment coefficient at zero angle of attack for each succeeding control deflection was used to compute the values of $C_{h\delta}$ shown in figure 9.

Longitudinal Trim and Force Coefficients

The variation of trim angle of attack with Mach number for the flight is shown in figure 10; this is a basic measurement and not a computed quantity. The figure shows an angle of attack about -2° when the canard

deflection was 0.4° . Since the model was essentially symmetric to the XY-plane, trim angle of attack near 0° could have been expected. There may have been a constant error in α of about -2.5° of unknown origin, especially in light of the trim normal-force coefficient which has values of 0.05 when $\alpha_{\text{trim}} = -2^\circ$. (See fig. 11.) Inasmuch as the instrument calibration for α used in the present test was found to be linear, zero-point error would not affect the slopes.

The normal-force curves of all model oscillations are presented in figure 12. The normal-force-curve slopes in figure 13 are compared with values of lift-curve slope predicted by Convair (originally presented in ref. 1) and with unpublished data. In general, the rocket model data show lower values than either of the two curves. No correction for flexibility was applied to the data to increase the values. The maximum recorded oscillation of angle of sideslip was 2.5° at $M = 2.46$, but no values were obtained at a Mach number less than 1.55. Observation of the sidewise acceleration indicated that 2.5° was the largest angle of sideslip in the flight.

The same time intervals were used in the presentation of data for figures 12 and 14 such that both of the plots show the same 1 to 2 cycles of the longitudinal motion. The data presented in figure 14 are chord-force coefficient plotted against normal-force coefficient. The presentation of chord force obviates any necessity of assuming that the angle-of-attack instrument had or had not a shift of zero indication. The essentially constant values of C_c indicate that the increment in normal force due to a change in angle of attack is normal to the chord plane.

Stability

Figures 15 to 18 describe the longitudinal stability of the external store rocket model. In figure 15 is plotted the variation of the periods of the longitudinal motions with Mach number, and from these data the static stability derivative C_{m_α} shown in figure 16 was computed. Since a one-degree-of-freedom motion in pitch was assumed, the following equation was used:

$$C_{m_\alpha} = - \frac{0.688 I_y}{P^2 q S \bar{c}}$$

The dynamic stability is depicted in figure 17 as the time in which the longitudinal motions damp to one-half amplitude. The pitch damping

derivative $C_{m_q} + C_{m_{\dot{\alpha}}}$ was found from the equations for a two-degree-of-freedom motion in pitch. The variation of this derivative with Mach number is shown in figure 18. The model, which has its center of gravity located 2.874 feet behind the nose, is shown to be statically and dynamically stable.

SUMMARY OF RESULTS

A longitudinal stability and control investigation made over a Mach number range from 0.94 to 2.58 of a 1/7-scale model of an external store indicated the following results:

1. Hinge moments of an all-movable canard control surface were small at supersonic speeds. This fact indicated that the hinge line was near the center of pressure. The variation of hinge moment with angle of attack decreased rapidly as Mach number increased from 0.94 to about 1.2 but was more nearly constant at higher Mach numbers.
2. A significant constant shift in the recording of angle of attack was suspected and this error chiefly affected the trim values and not the slopes.
3. Most of the pitching motions were too small for good accuracy but the normal-force-curve slope was found to be slightly less than the lift-curve slope predicted in NACA Research Memorandum SL55G22a.
4. For a center of gravity 2.874 feet behind the nose, the model was statically and dynamically stable.

Langley Aeronautical Laboratory,
National Advisory Committee for Aeronautics,
Langley Field, Va., June 2, 1958.

REFERENCE

1. Hopko, Russel N.: Drag Near Zero Lift of a 1/7-Scale Model of the Convair B-58 External Store as Measured in Free Flight Between Mach Numbers of 0.8 and 2.45. NACA RM SL55G22a, U. S. Air Force, 1955.

TABLE I.- PHYSICAL CHARACTERISTICS

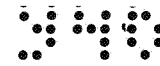
Wing:	
Area, sq ft	2.860
Span, ft	2.449
Mean aerodynamic chord, ft	1.557
Leading-edge sweep, deg	60
Trailing-edge sweep, deg	-10
Aspect ratio	2.097
NACA airfoil section	0004.5-64
Dihedral angle, deg	0
Incidence angle, deg	0
Canard:	
Area, sq ft	0.846
Span (total), ft	1.332
Mean aerodynamic chord of total canard surface, ft	0.848
Leading-edge sweep, deg	60
Trailing-edge sweep, deg	-10
Aspect ratio	2.096
NACA airfoil section	0005-64
Dihedral angle	0
Exposed area, sq ft	0.341
Mean aerodynamic chord of exposed canard surface, \bar{c}_s , ft	0.631
Hinge line, percent \bar{c}_s	53
Vertical tail:	
Lower fin -	
Area to body center line, sq ft	0.613
Leading-edge sweep, deg	60
Aspect ratio	1.749
Taper ratio	0.349
Height below center line, ft	0.732
Upper fin -	
Area to body center line, sq ft	0.552
Leading-edge sweep, deg	60
Aspect ratio	2.170
Taper ratio	0.334
Height below center line, ft	-0.774
Body:	
Length, ft	7.322
Maximum diameter, ft	0.714
Mass data:	
Weight, lb	212.8
Center-of-gravity location rearward of nose, ft	2.874
Mass	6.652
Center-of-gravity height below center line, ft	0.0213
I_x , ft-lb-sec ²	0.503
I_y , ft-lb-sec ²	21.5
I_z , ft-lb-sec ²	21.9
Inclination of principal axis	0

TABLE II.- ACCURACY OF QUANTITIES

δ , percent	± 2
H, in-lb	± 15
W, percent	± 0.5
I_X , percent	± 4.0
I_Y , percent	± 2.0
I_Z , percent	± 2.0
$\alpha - \alpha_{trim}$, deg	± 0.15
$C_{N\alpha}$, percent	± 5
$C_{m\alpha}$, percent	± 9
$C_{mq} + C_{m\dot{\alpha}}$, percent	± 25

	M = 1.1	M = 2.5
M, percent	± 1.5	1.0
q, percent	± 3.0	2.0
C_N	± 0.007	0.003
C_c	± 0.11	0.05
P, sec	± 0.006	0.003
$t_{0.5}$, sec	± 0.06	0.03





CONFIDENTIAL

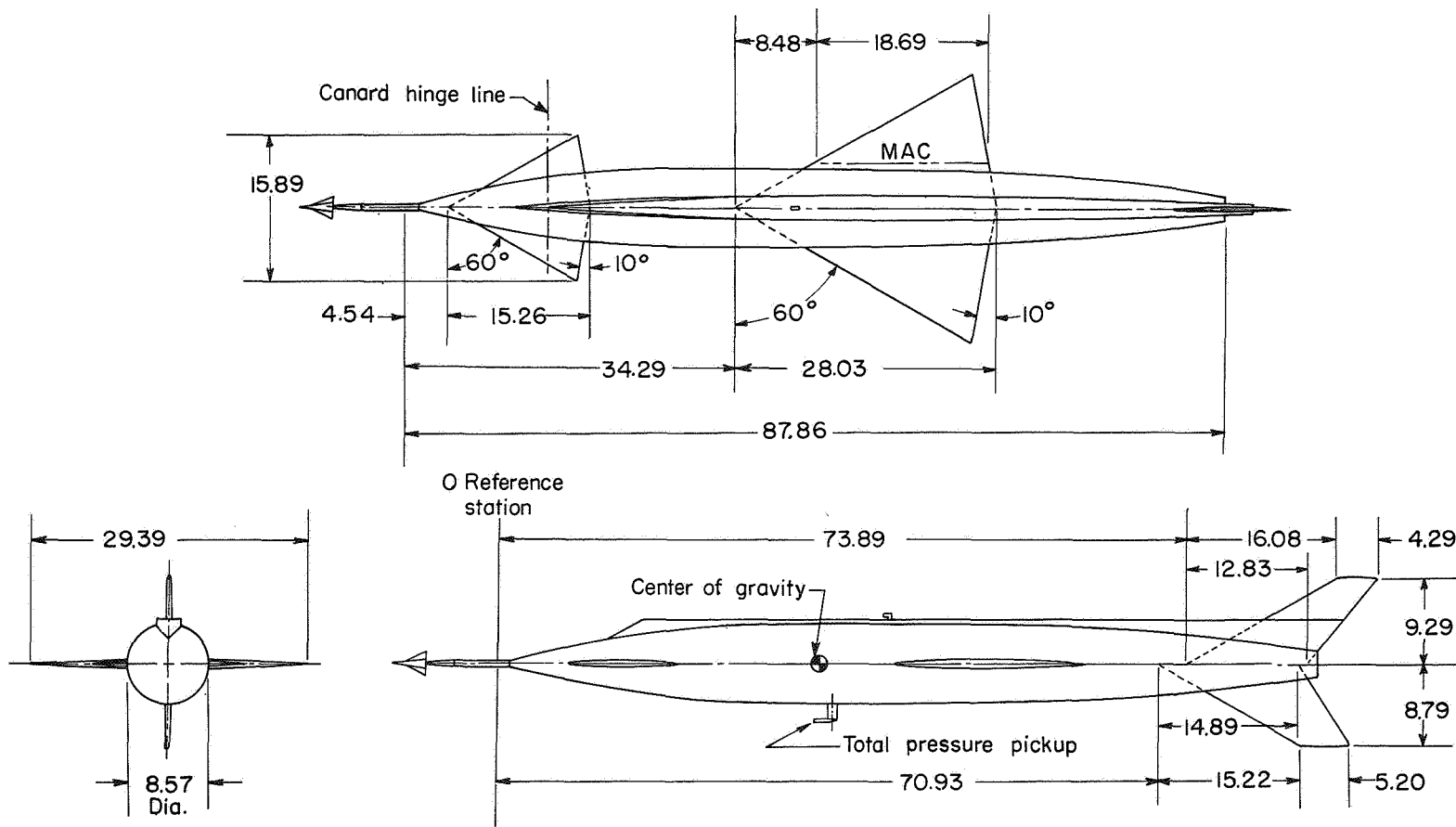


Figure 1.- Three-view drawing of 1/7-scale model of B-58 external store. Linear dimensions in inches.

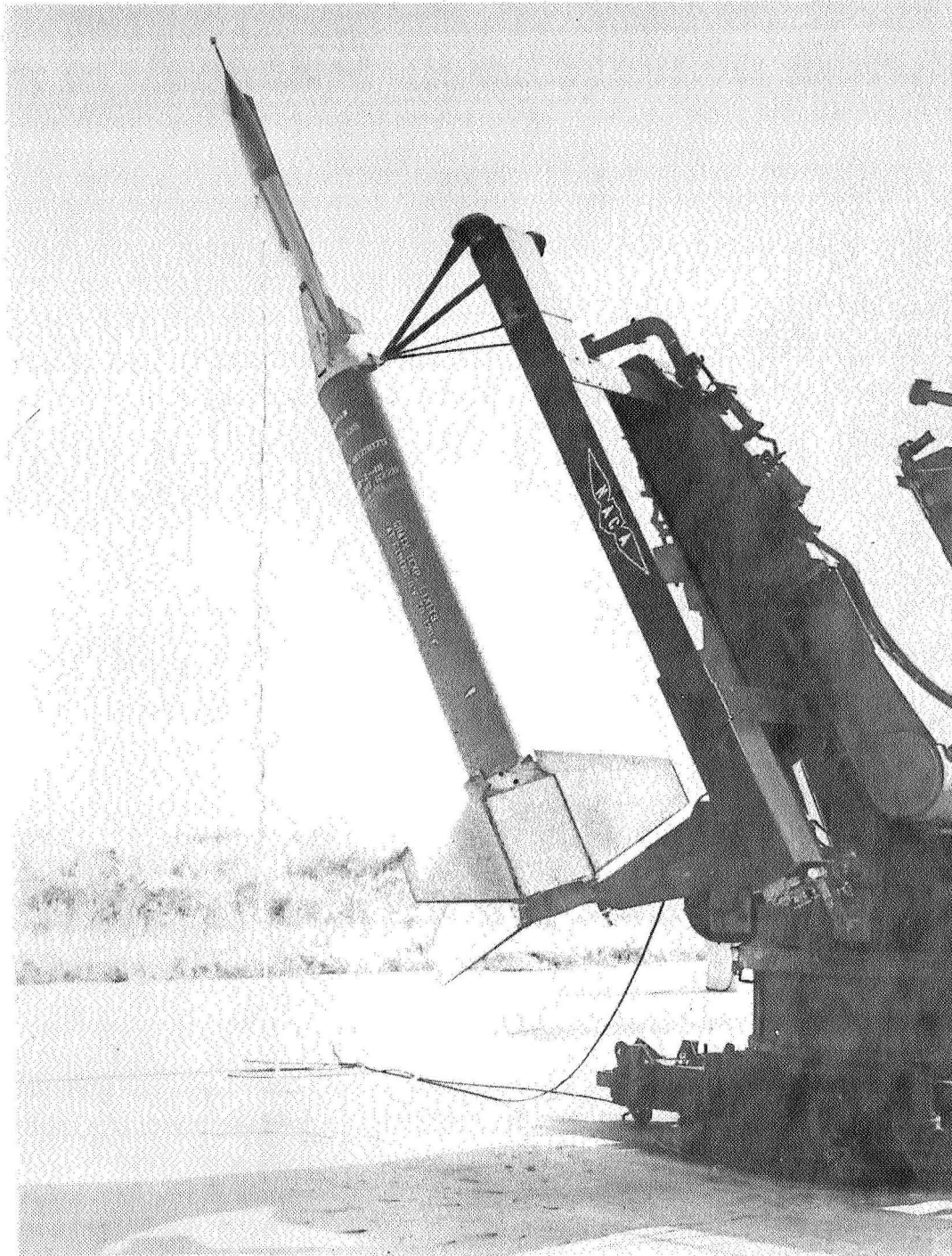


Figure 2.- Photograph of model and booster on launcher: L-96110.1

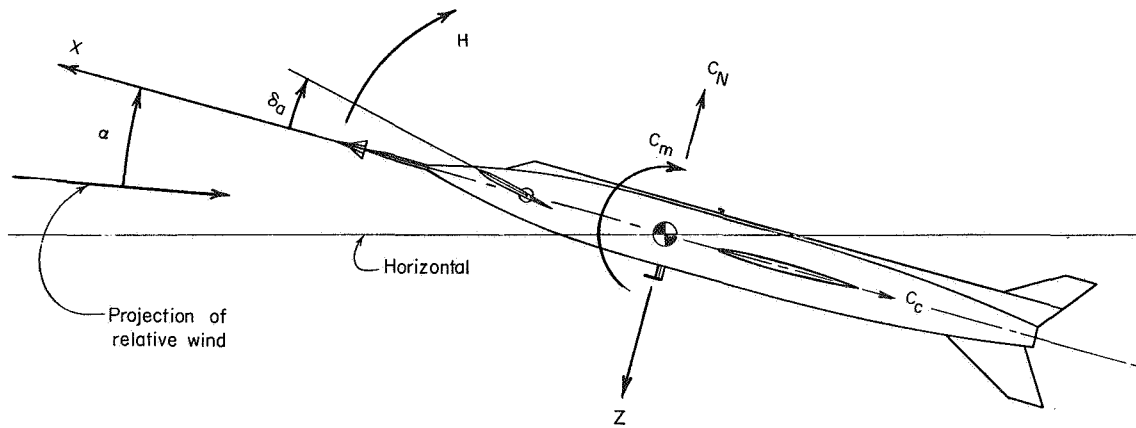


Figure 3.- Sketch of model showing body system of axes used in the investigation and the positive directions of forces, moments, and angles.

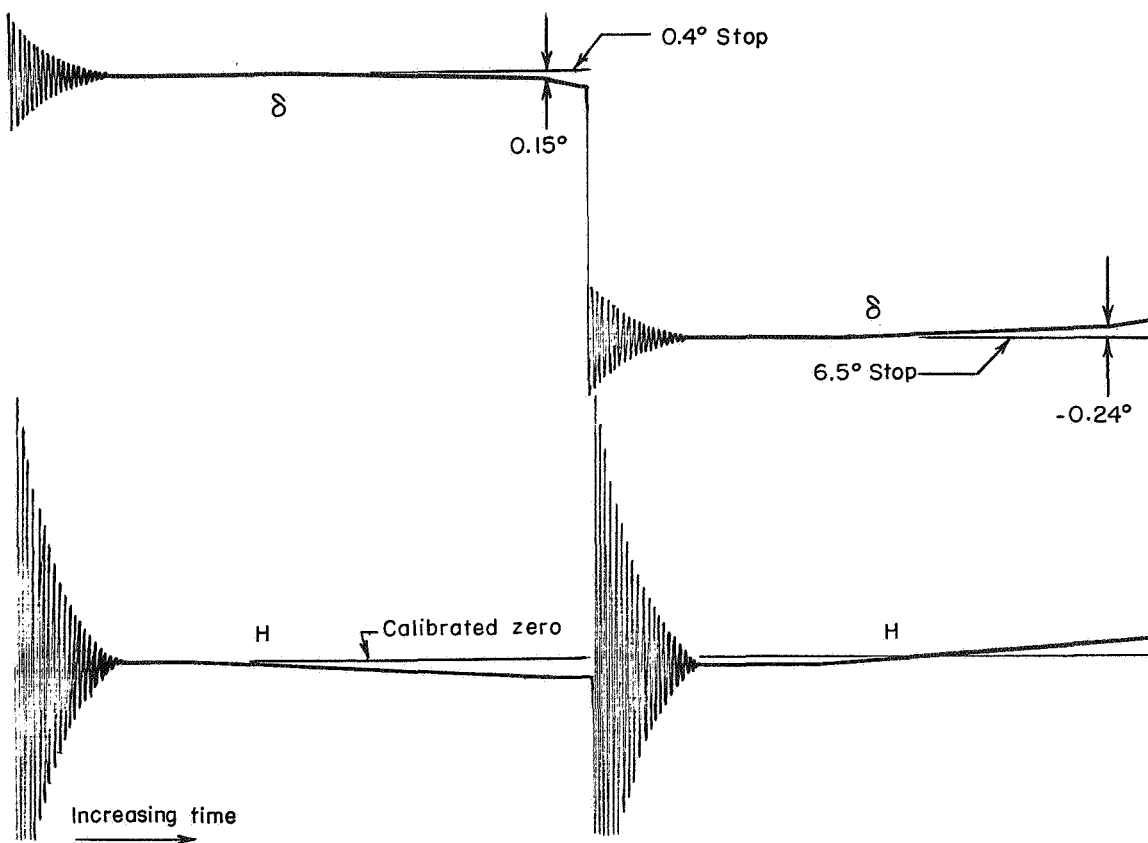
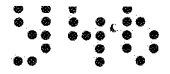


Figure 4.- Sample time history of preflight record of control pulse showing the effect of internal actuator forces on the measured values of control deflection and hinge moment. No externally applied hinge moments.



CONFIDENTIAL

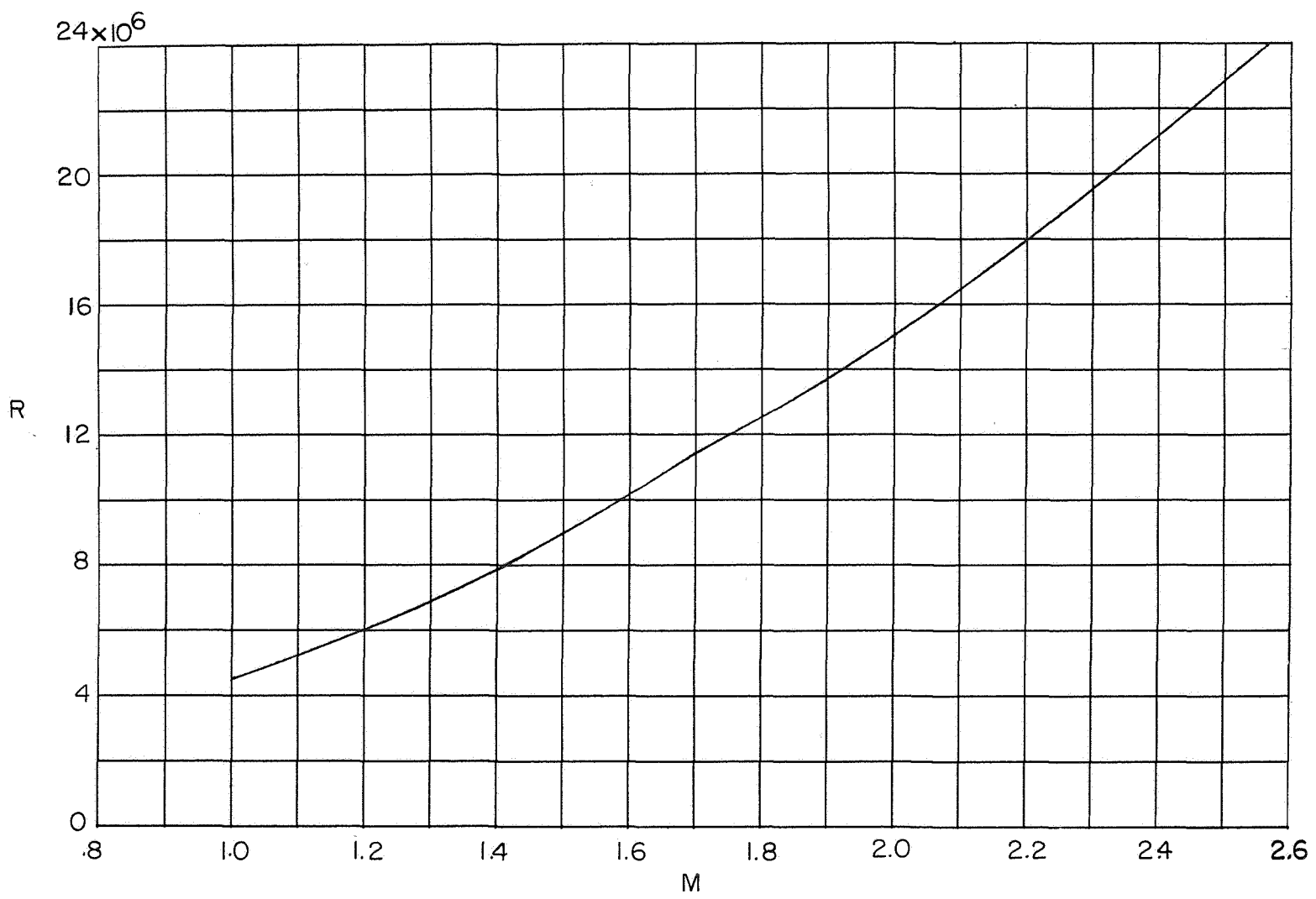


Figure 5.- Test Reynolds number.

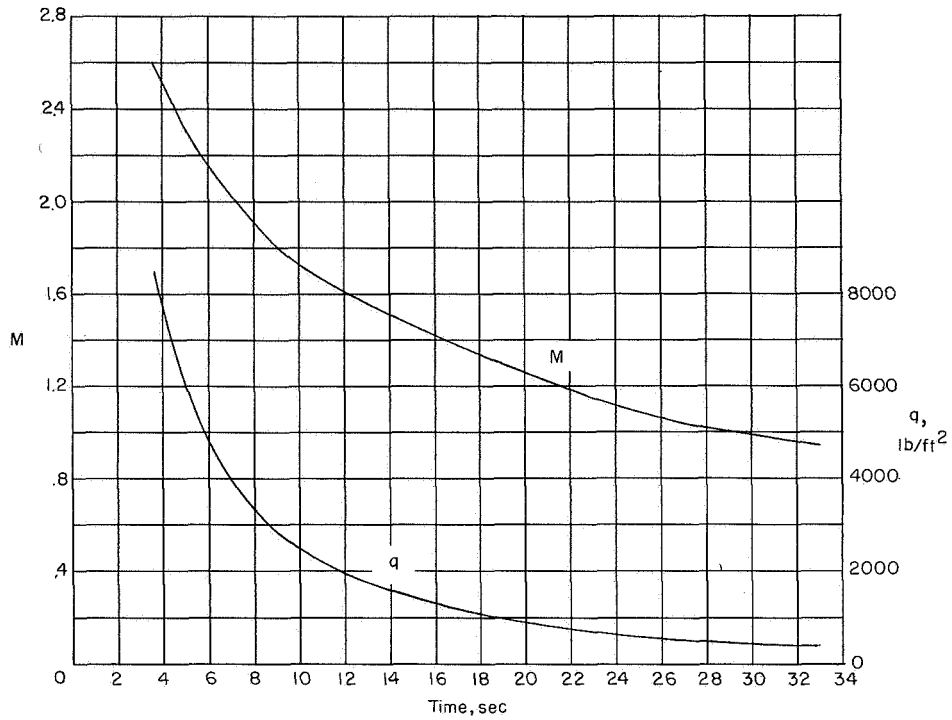


Figure 6.- Time histories of Mach number and dynamic pressure.

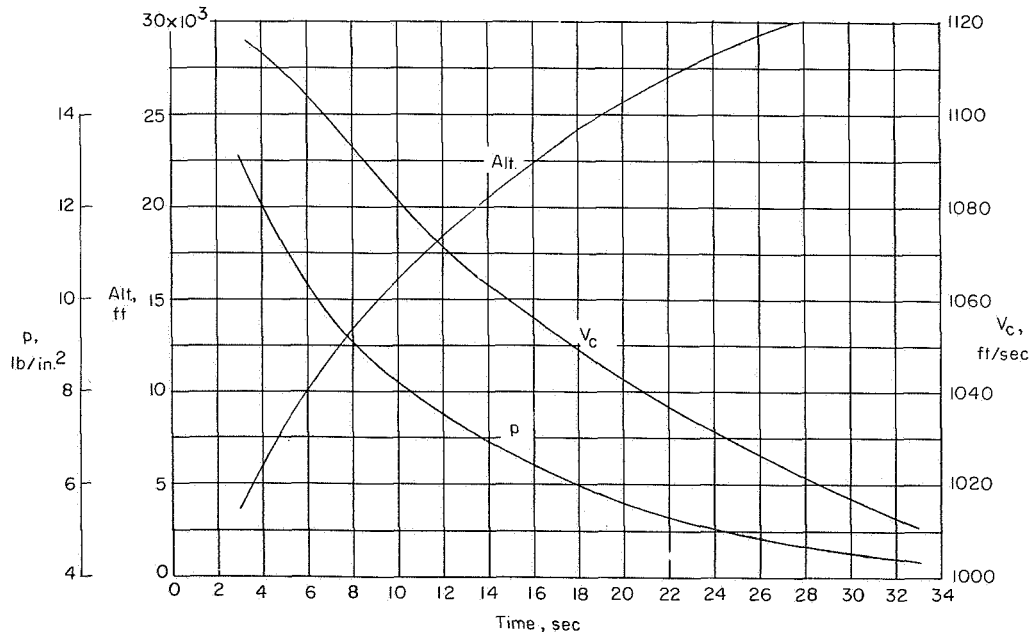


Figure 7.- Time histories of altitude, speed of sound, and static pressure.



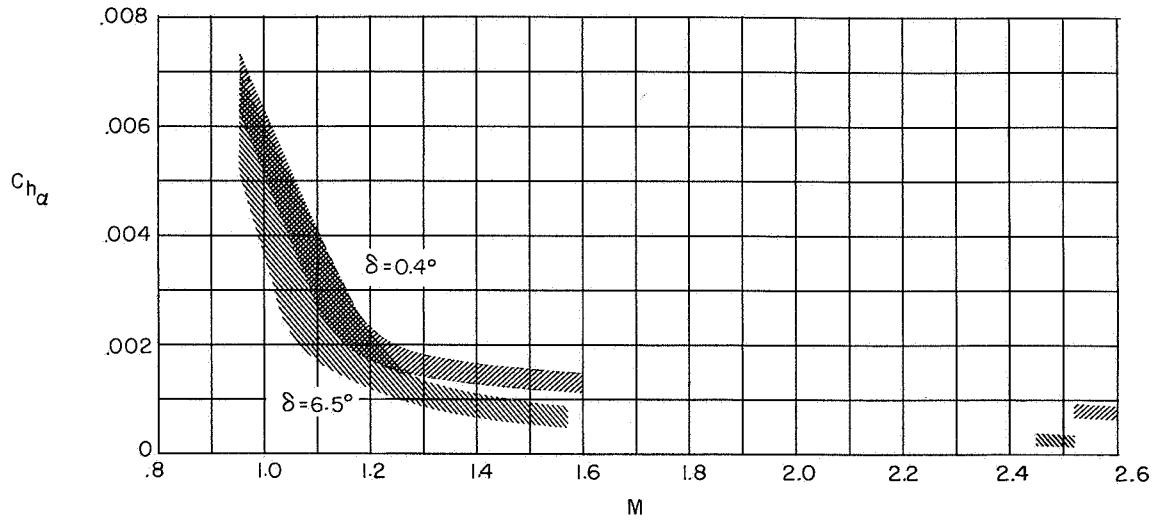


Figure 8.- Variation of $C_{h\alpha}$ with Mach number.

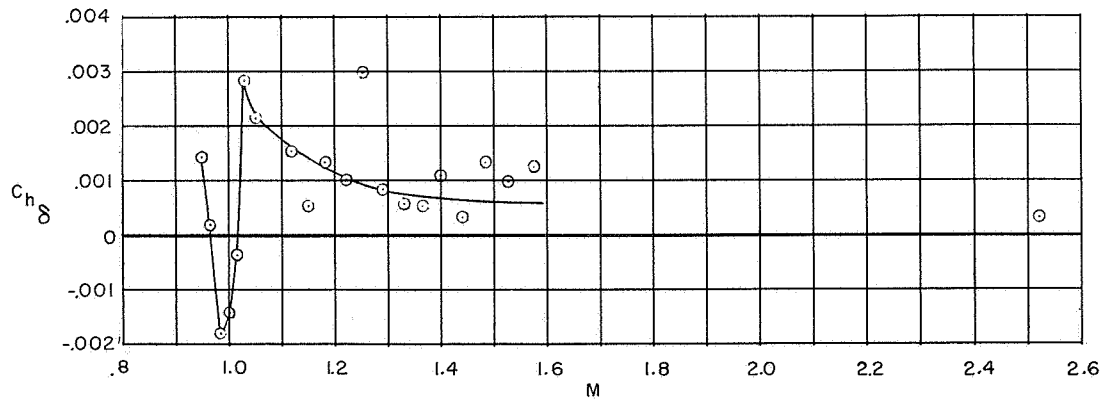
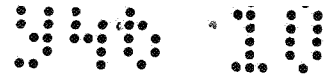


Figure 9.- Variation of $C_{h\delta}$ with Mach number.



CONFIDENTIAL

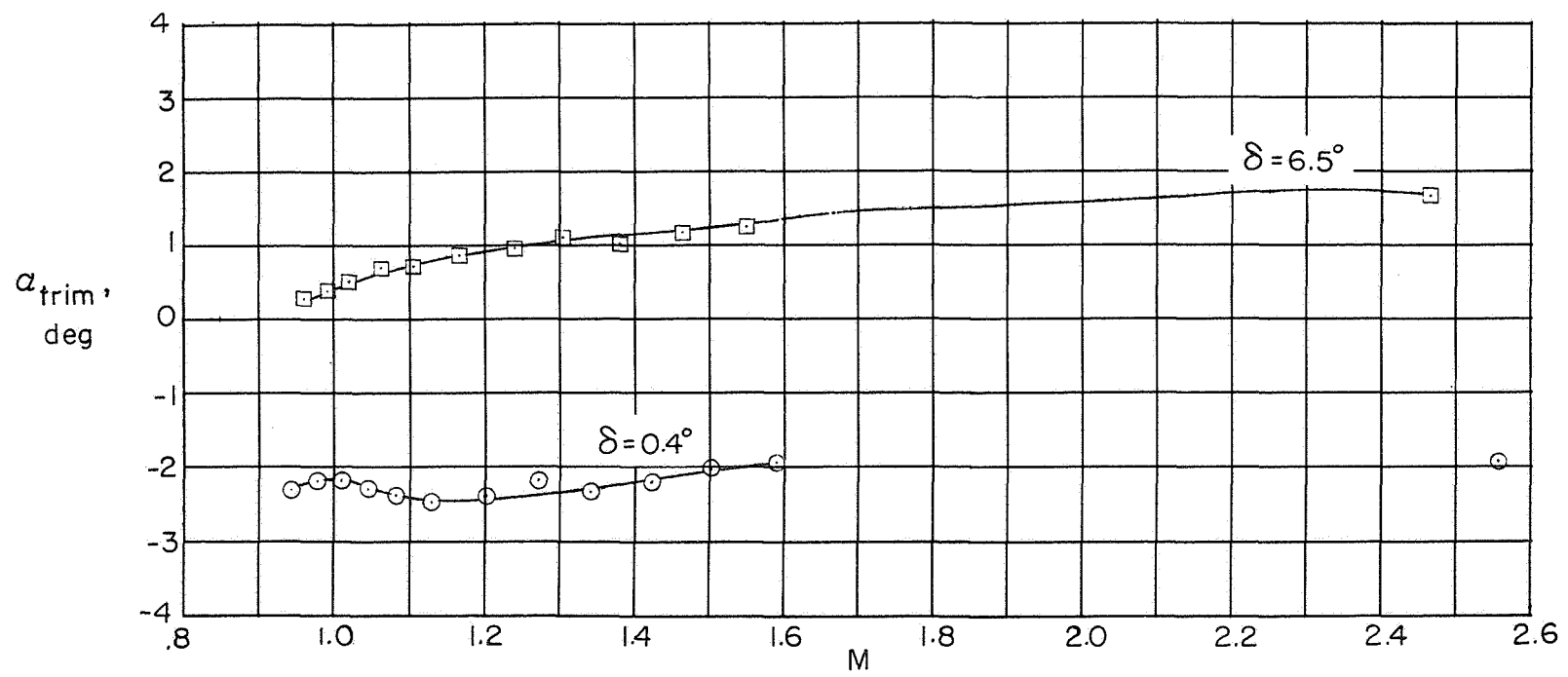
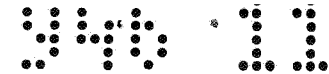


Figure 10.- Trim angle of attack.



CONFIDENTIAL

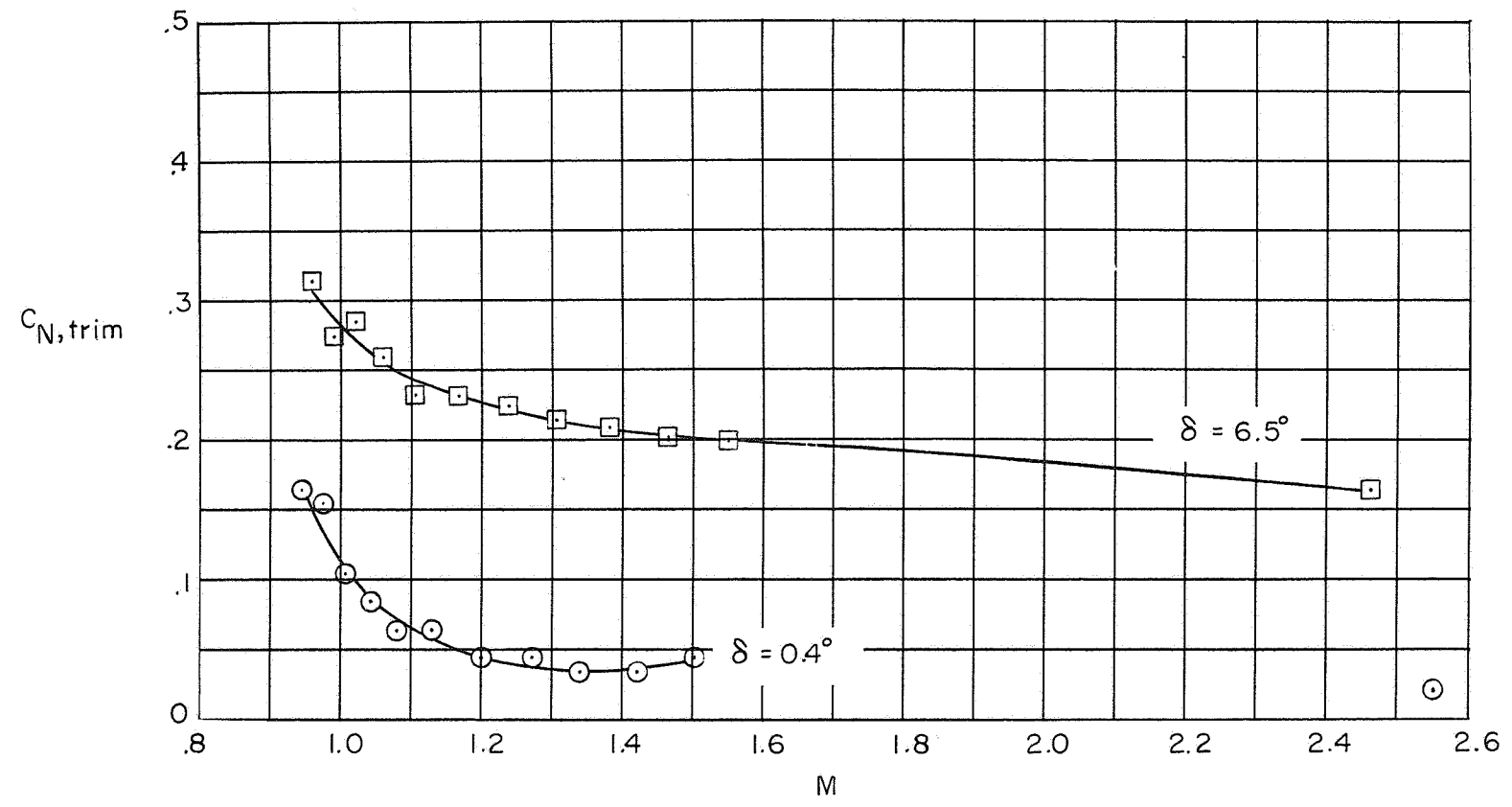
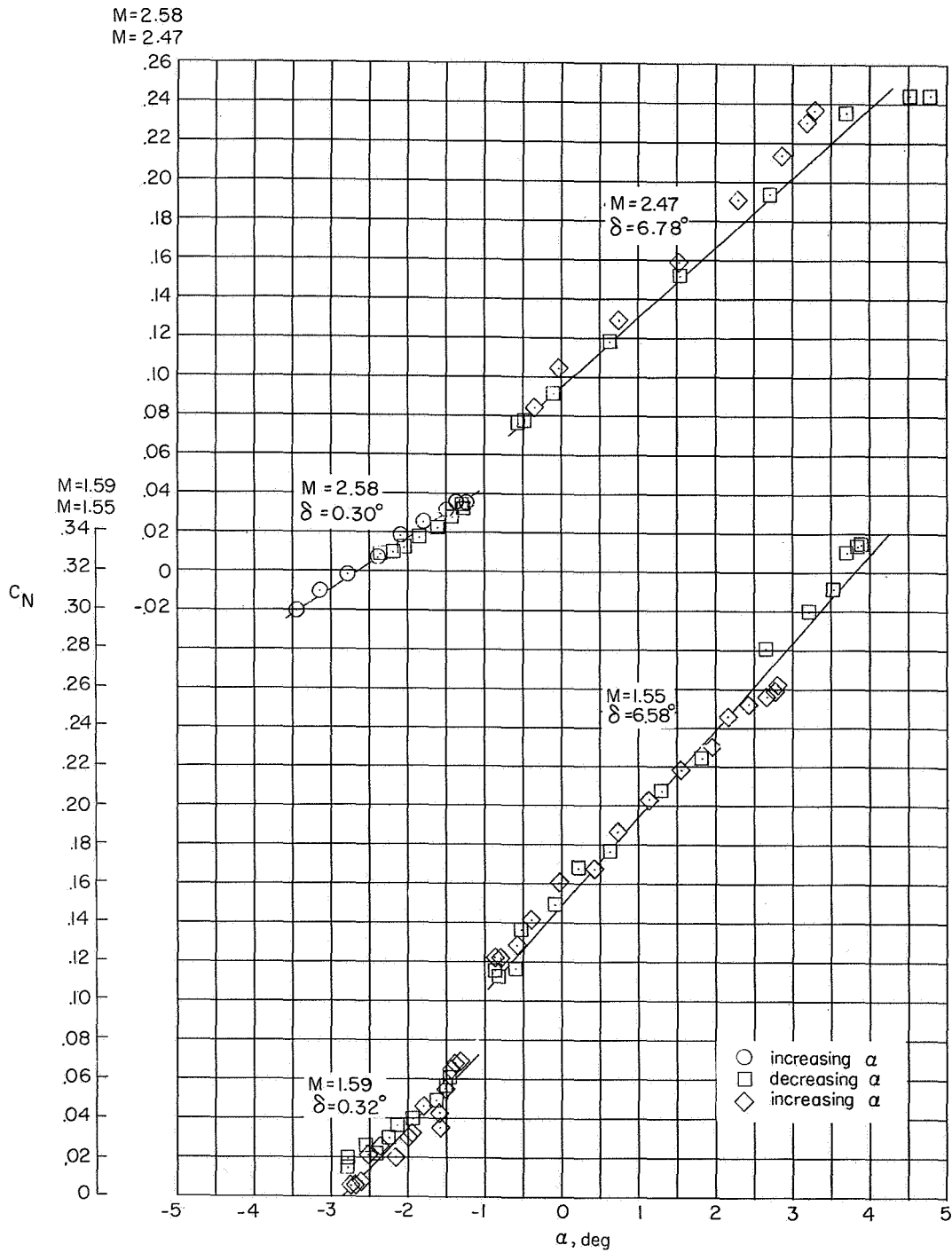
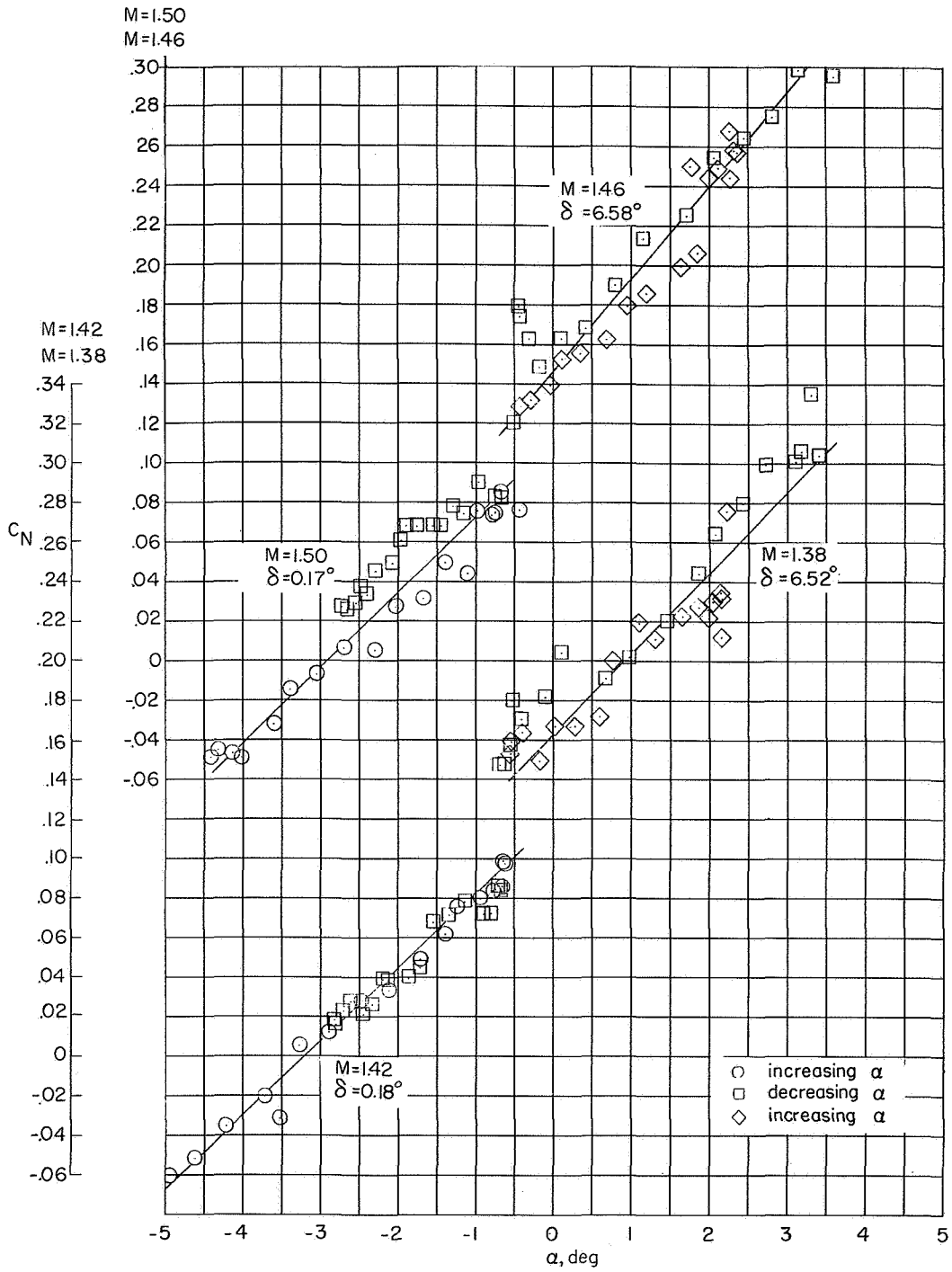


Figure 11.- Trim normal-force coefficient.



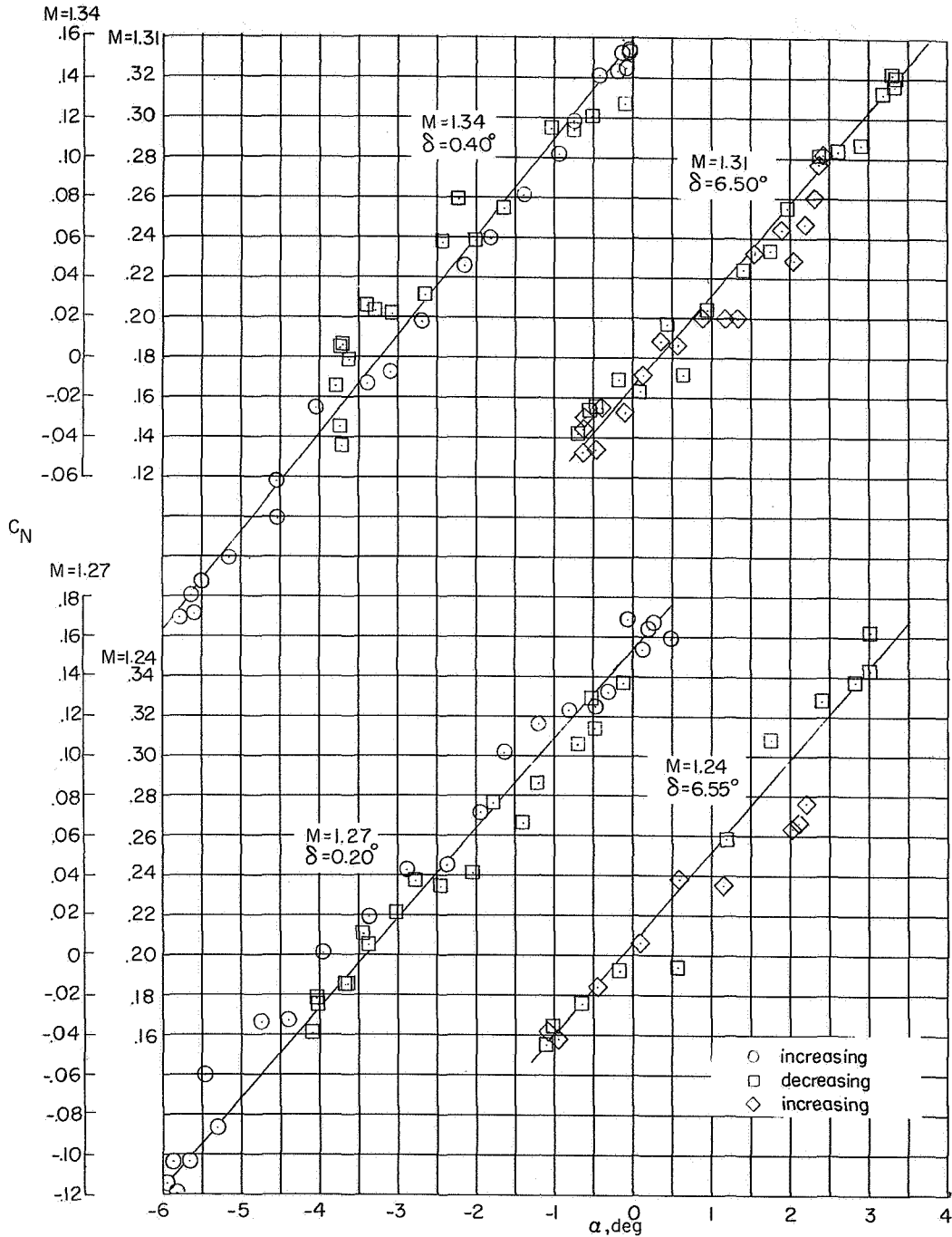
(a) $M = 2.58, 2.47, 1.59, \text{ and } 1.55$.

Figure 12.- Variation of normal-force coefficient with angle of attack.



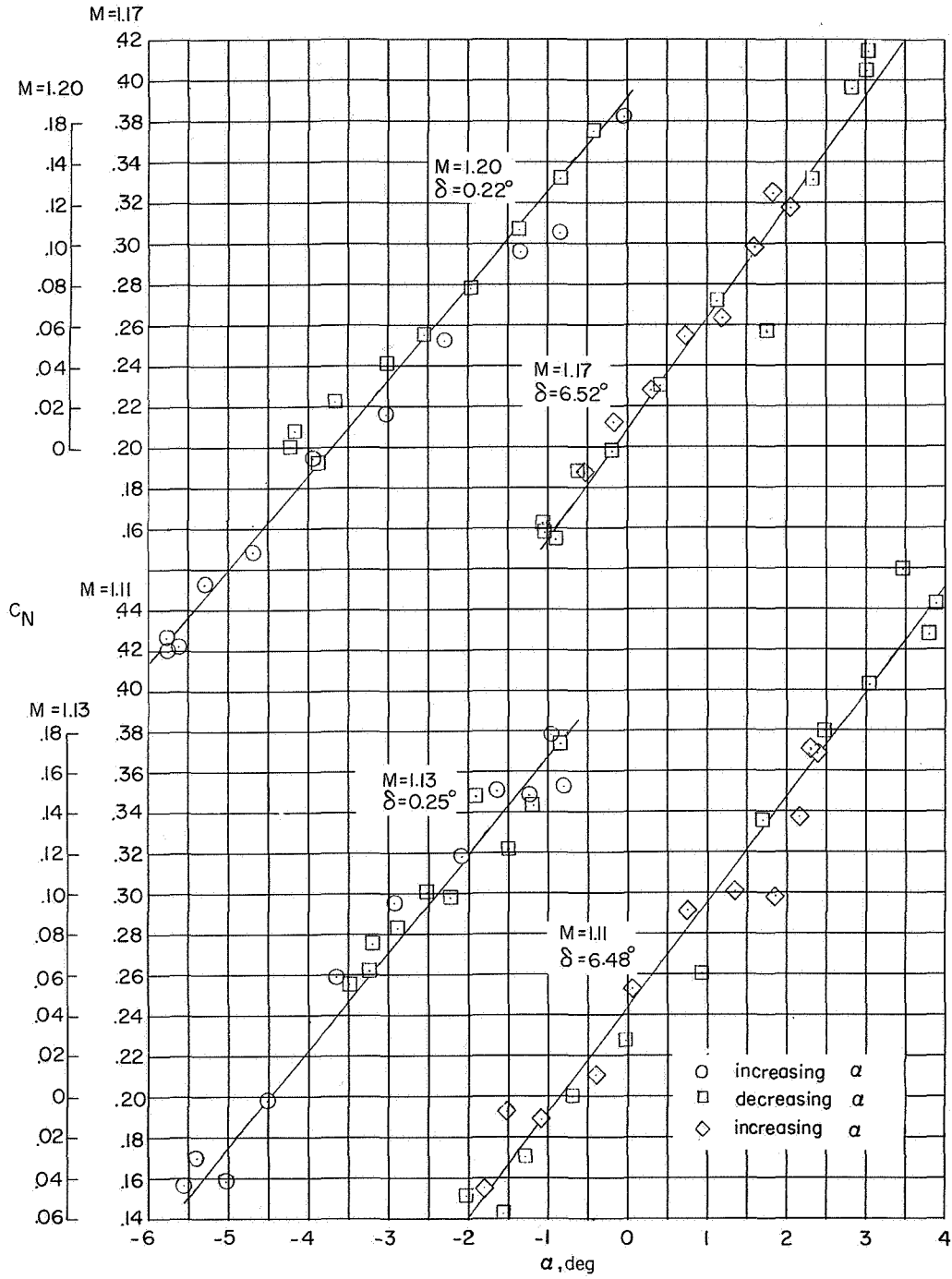
(b) $M = 1.50, 1.46, 1.42, \text{ and } 1.38.$

Figure 12.- Continued.



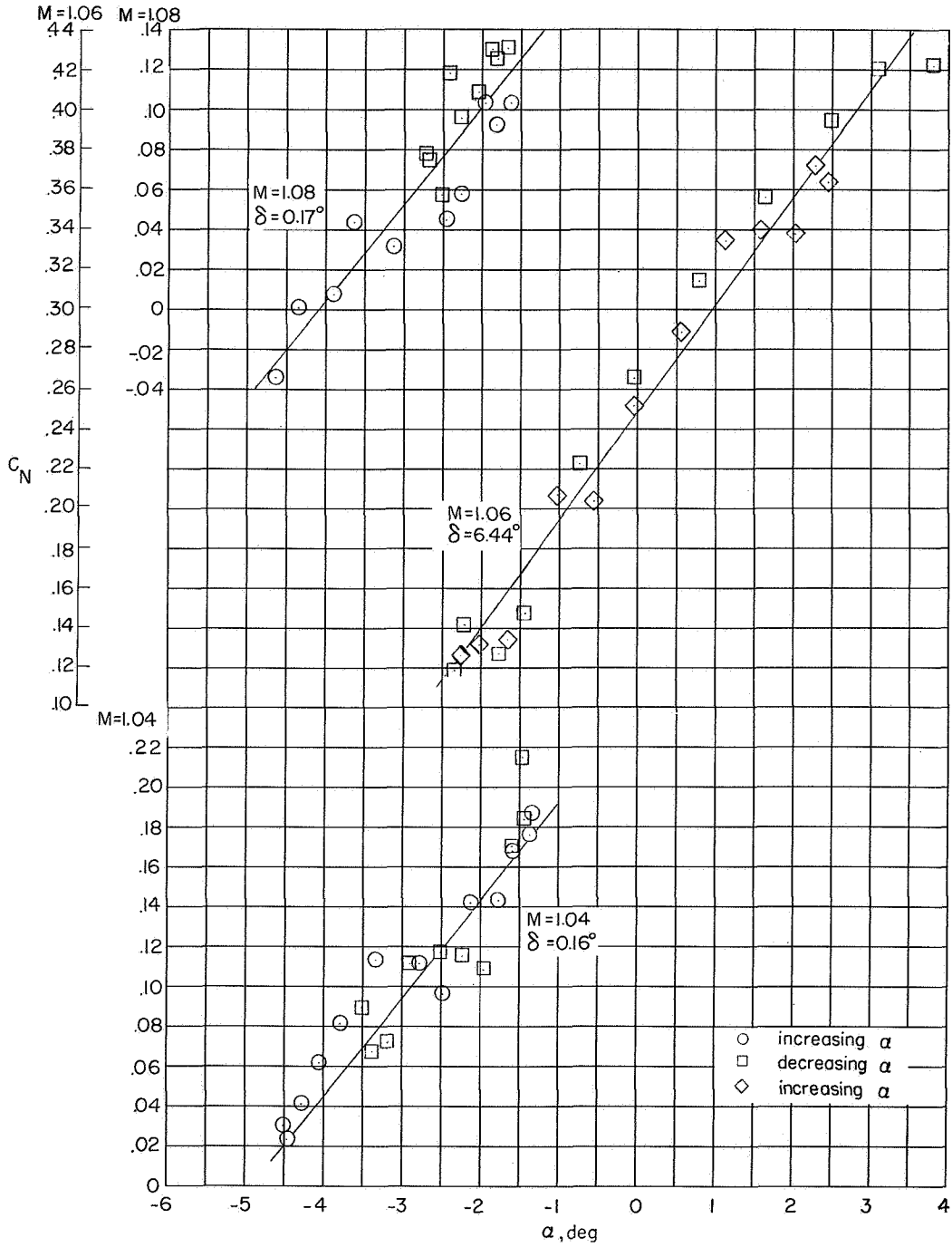
(c) $M = 1.34, 1.31, 1.27, \text{ and } 1.24.$

Figure 12.- Continued.



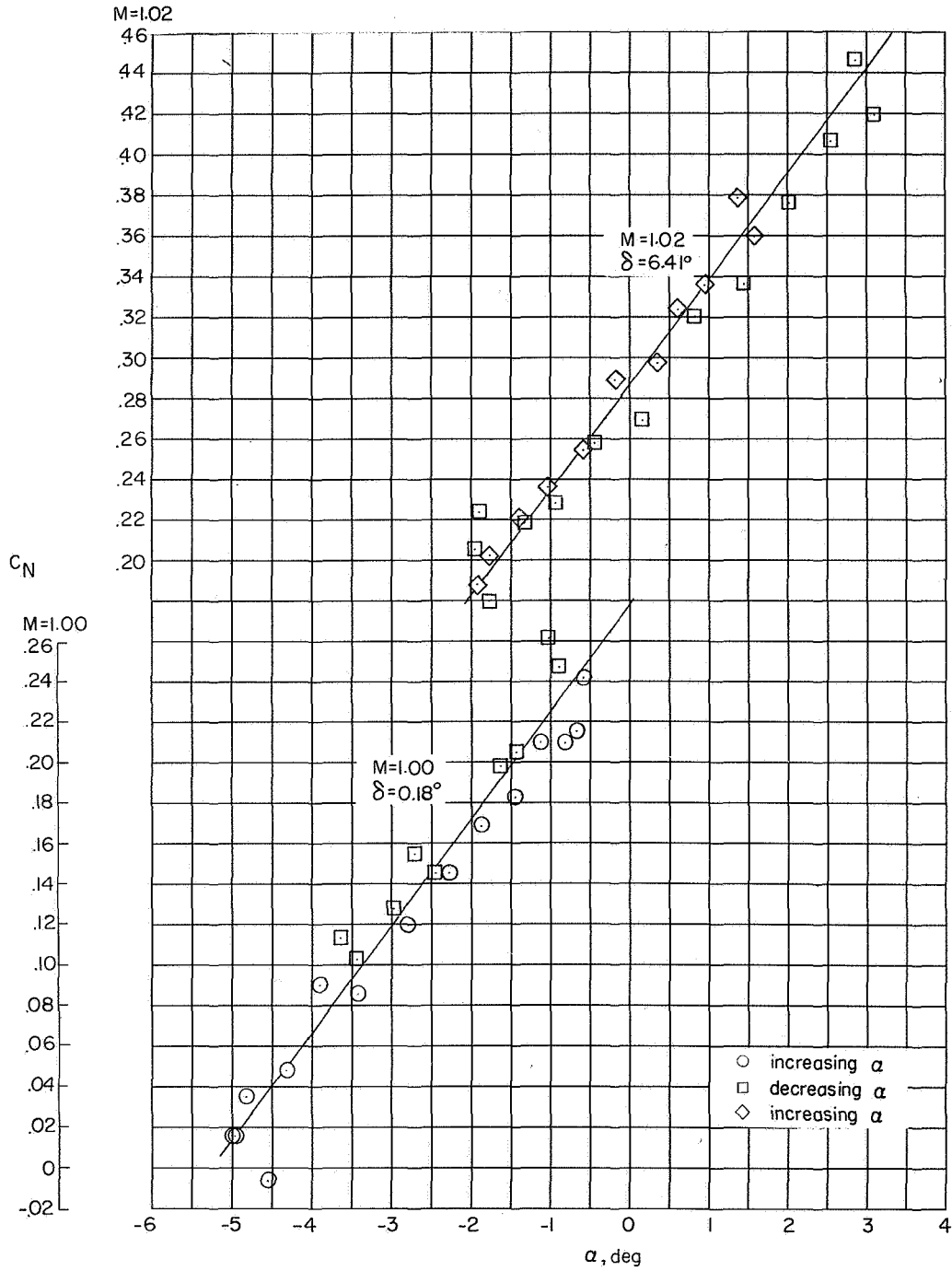
(d) $M = 1.20, 1.17, 1.13,$ and $1.11.$

Figure 12.- Continued.



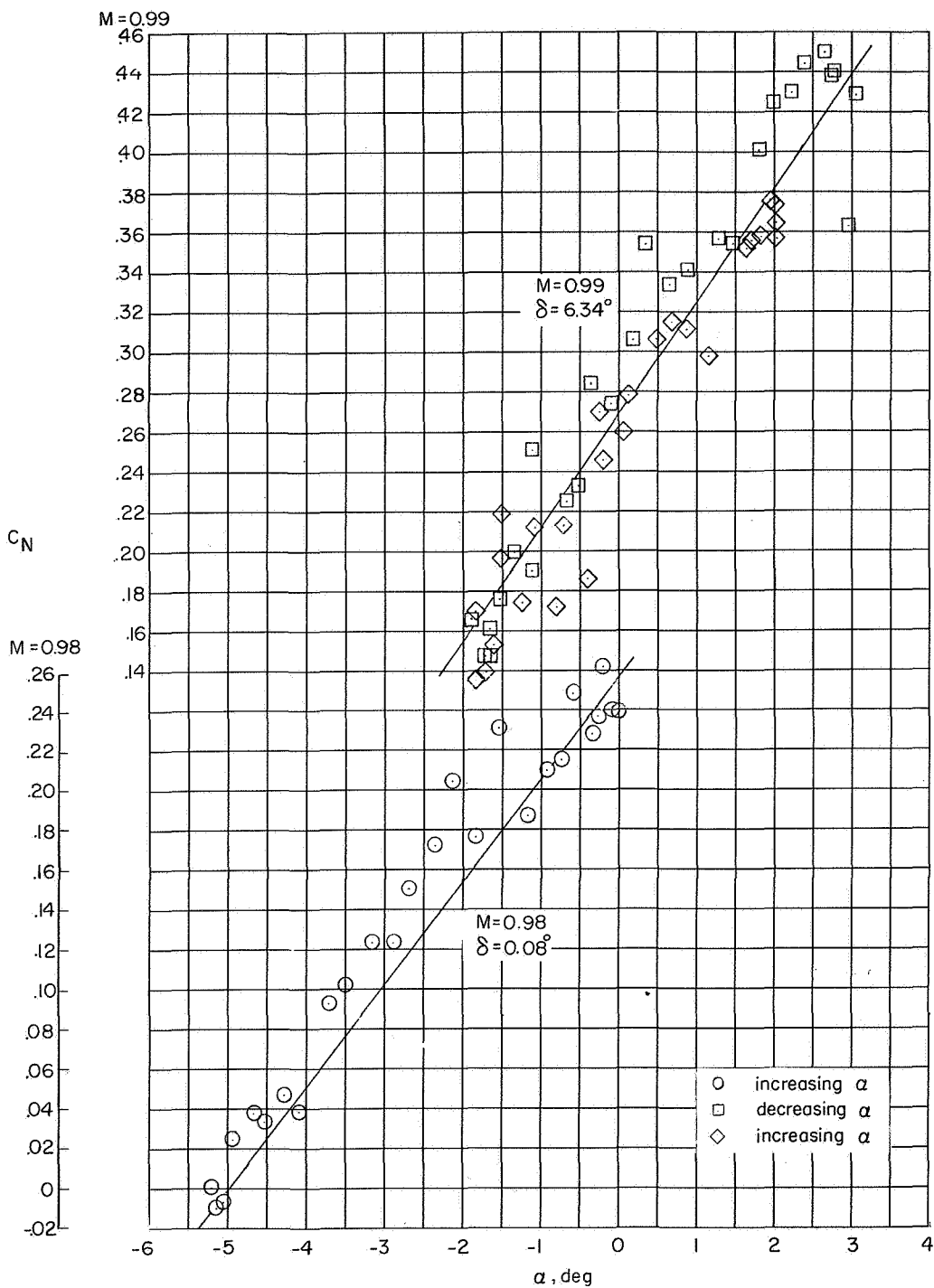
(e) $M = 1.08, 1.06, \text{ and } 1.04.$

Figure 12.- Continued.



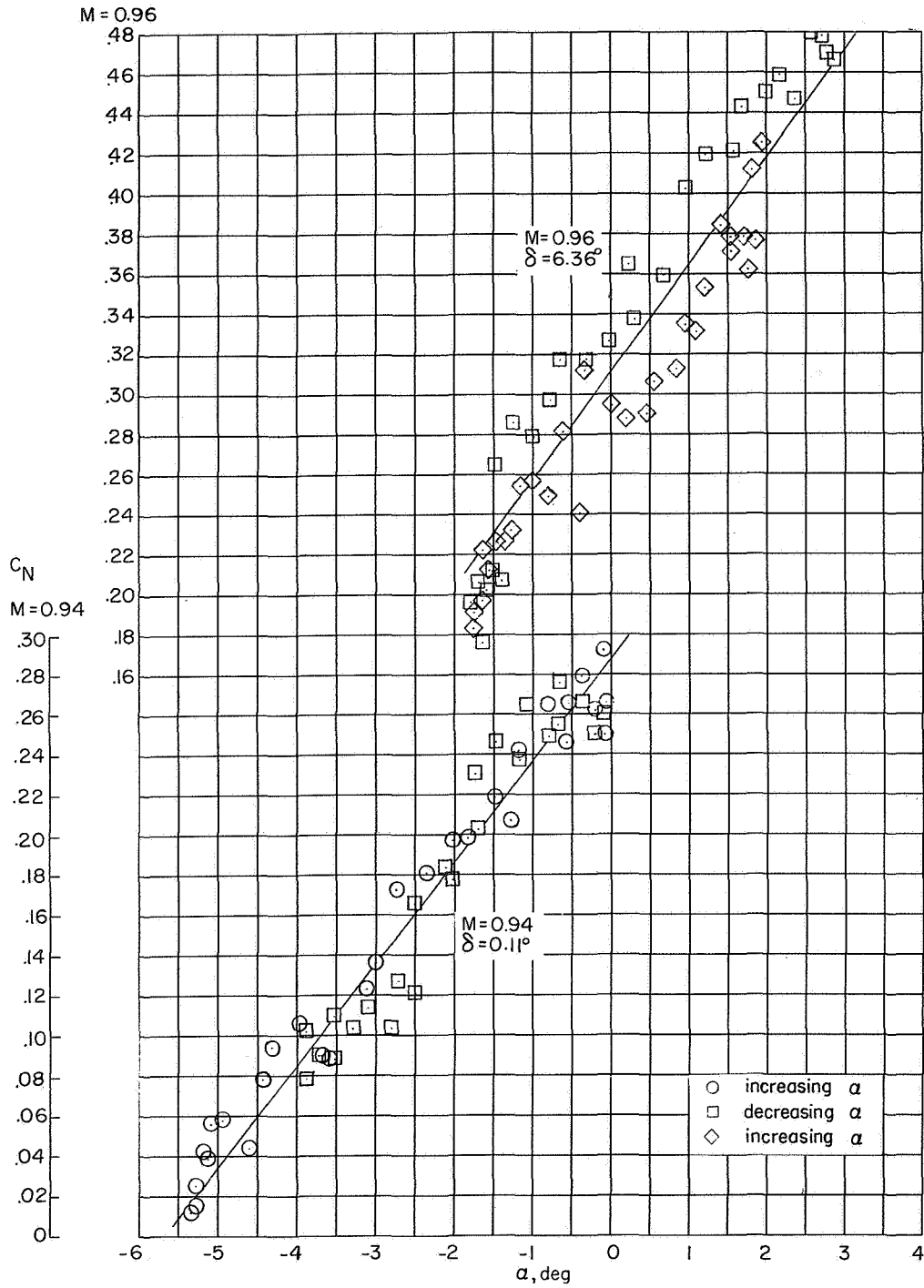
(f) $M = 1.02$ and 1.00 .

Figure 12.- Continued.



(g) $M = 0.99$ and 0.98 .

Figure 12.- Continued.



(h) $M = 0.96$ and 0.94 .

Figure 12.- Concluded.

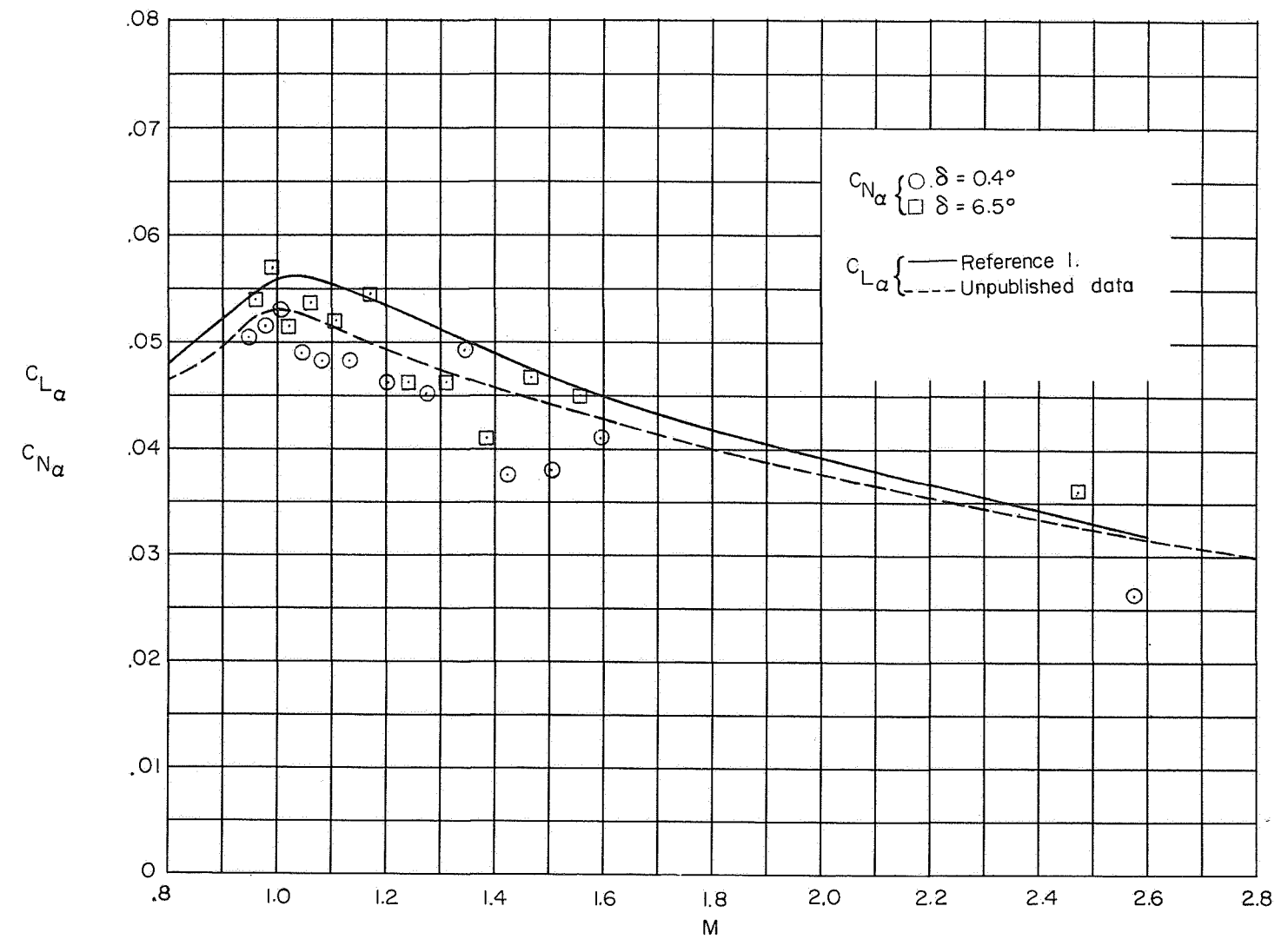
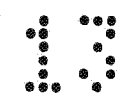
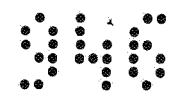
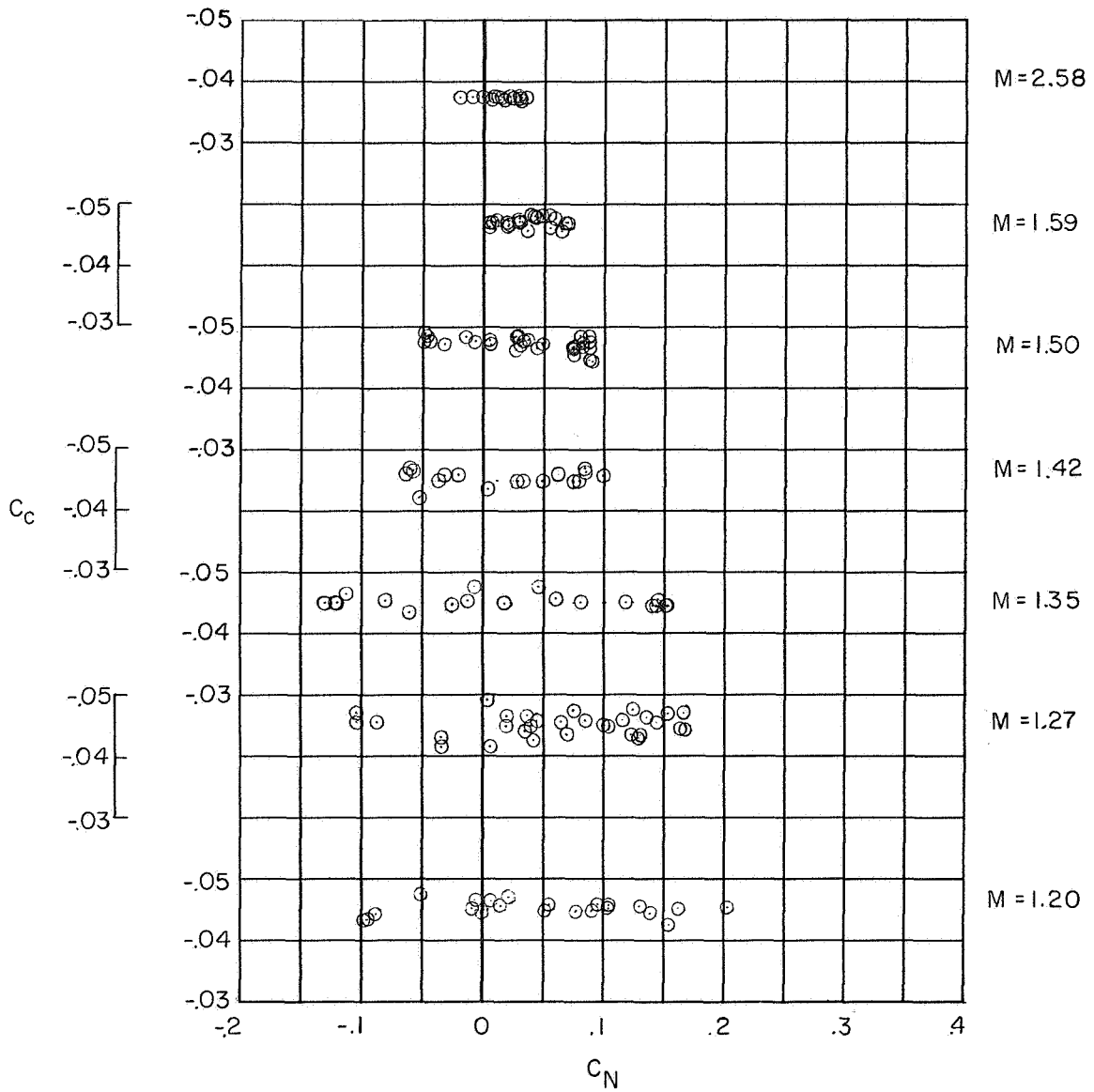
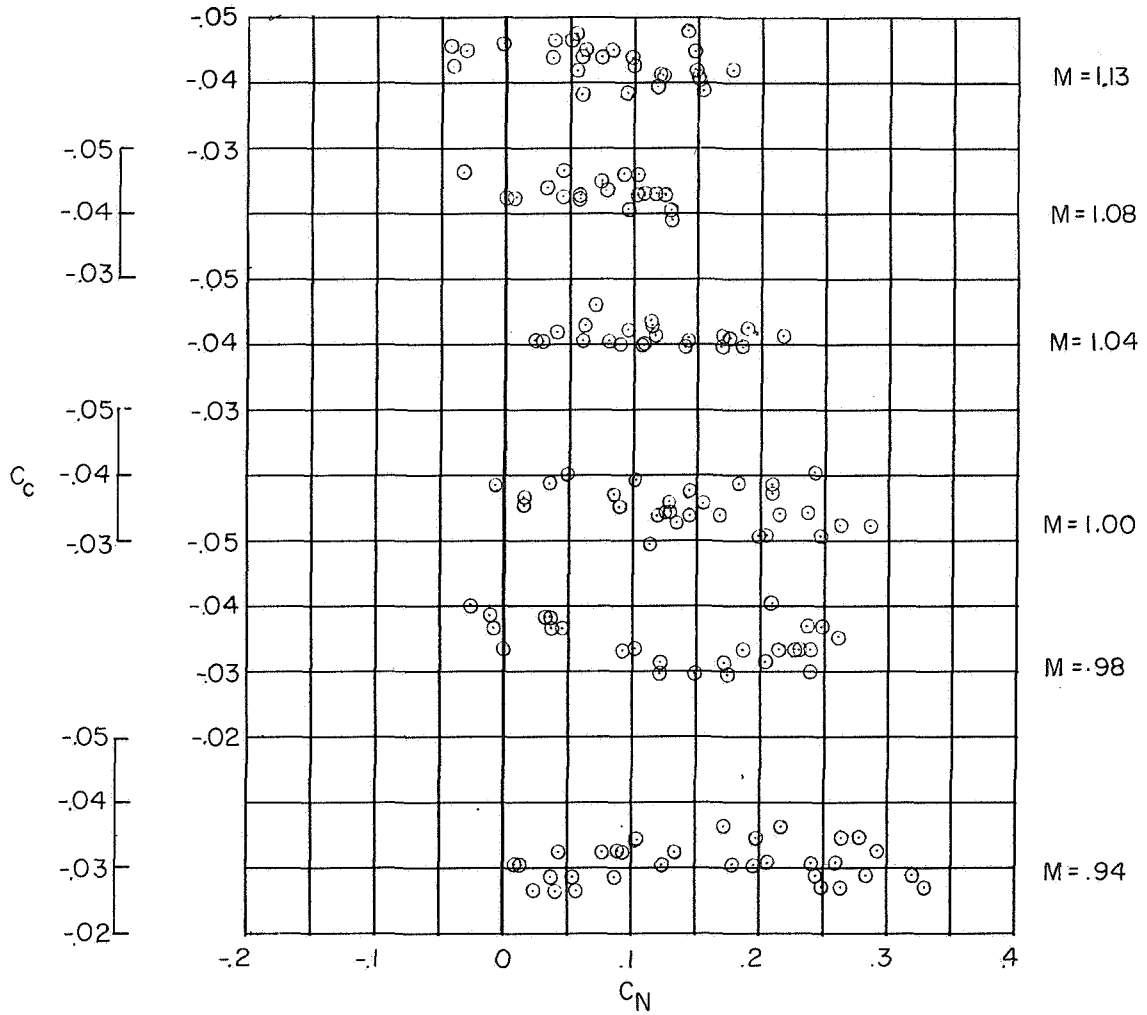


Figure 13.- Normal-force-curve slope of the model and reference lift-curve slopes.



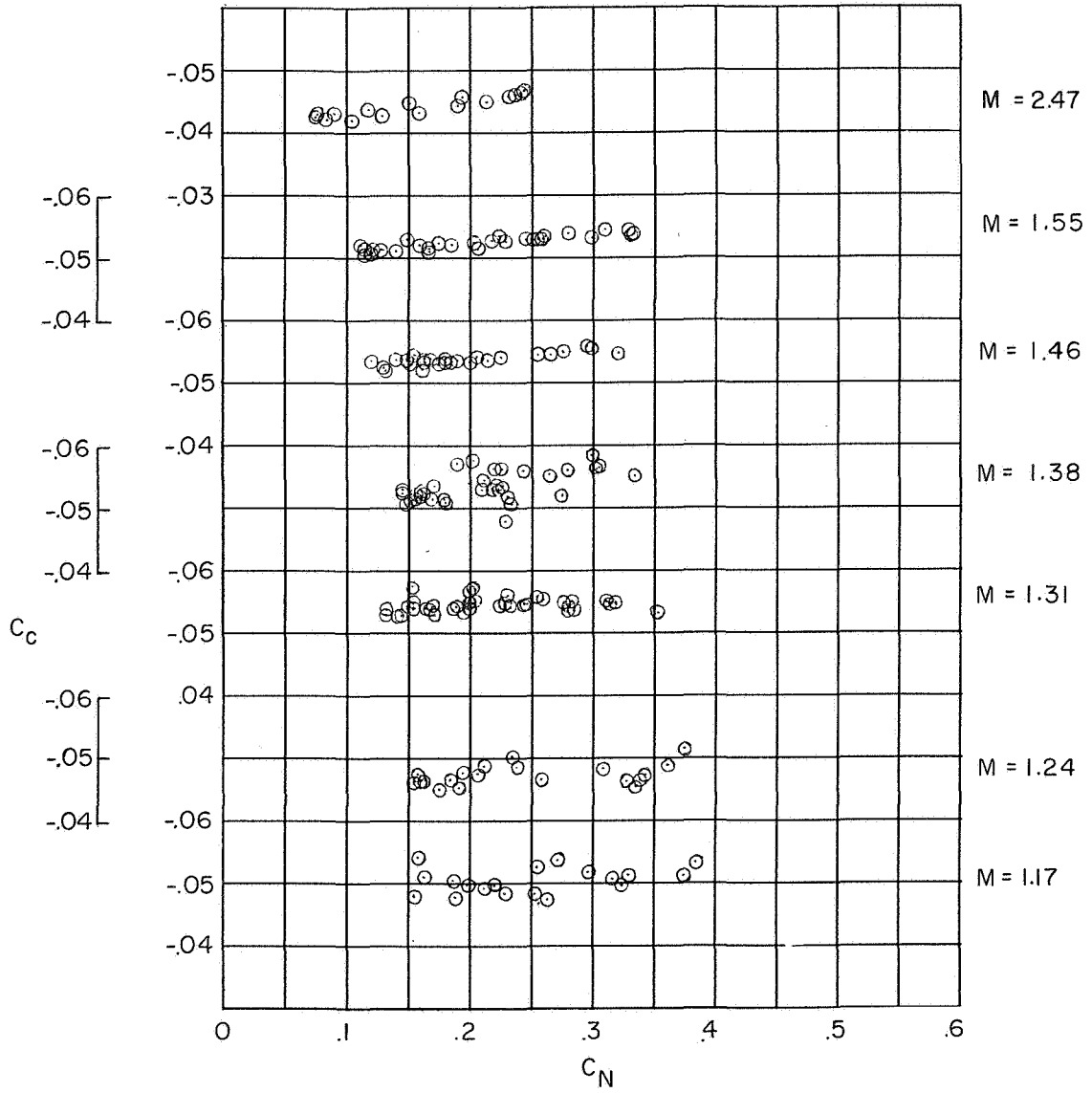
(a) $M = 1.20$ to 2.58 ; $\delta \approx 0.20^\circ$.

Figure 14.- Variation of chord-force coefficient with normal-force coefficient at each control position.



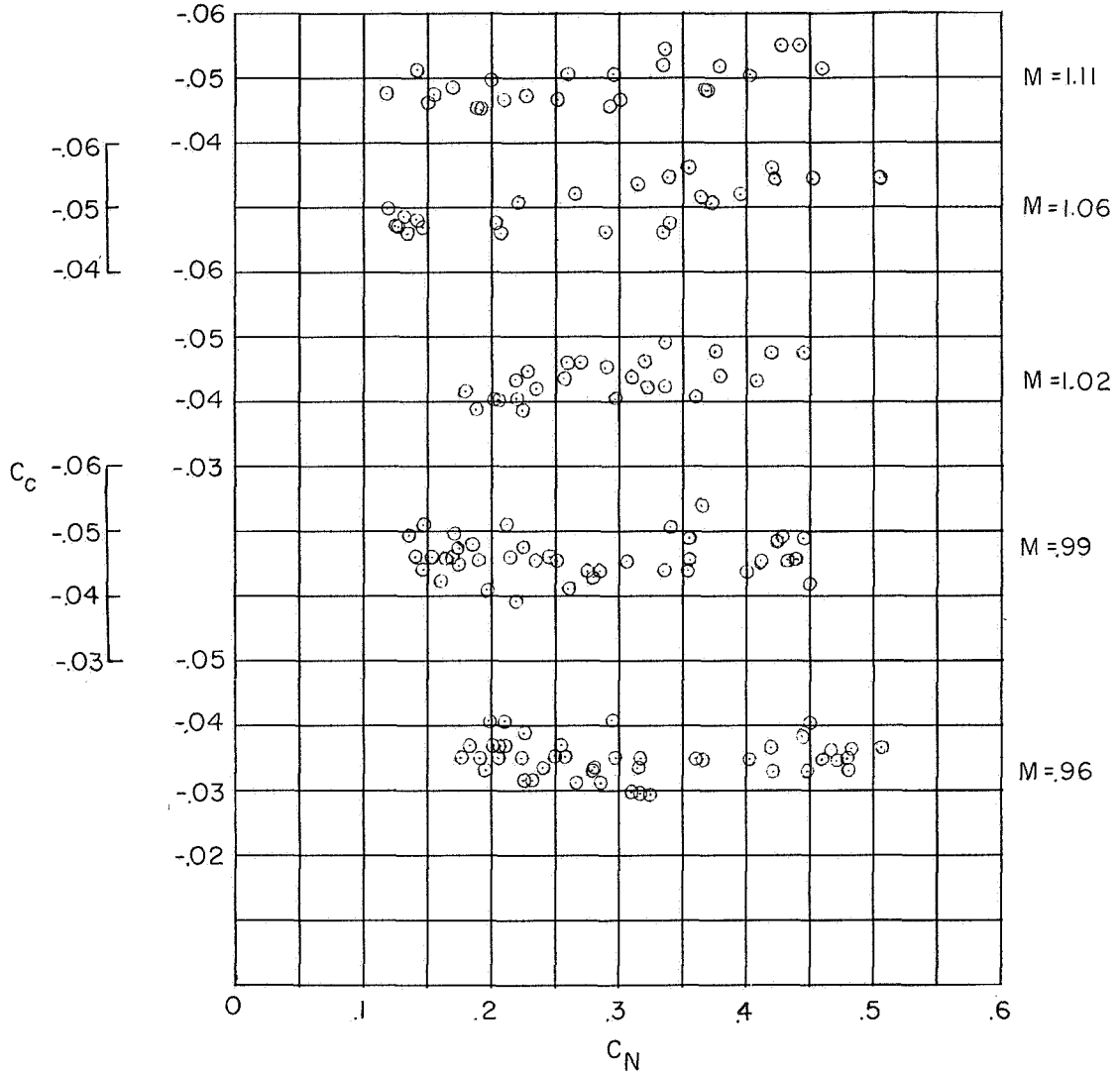
(b) $M = 0.94$ to 1.13 ; $\delta \approx 0.16^\circ$.

Figure 14.- Continued.



(c) $M = 1.17$ to 2.47 ; $\delta \approx 6.6^\circ$.

Figure 14.- Continued.



(d) $M = 0.96$ to 1.11 ; $\delta \approx 6.4^\circ$.

Figure 14.- Concluded.

CONFIDENTIAL

CONFIDENTIAL

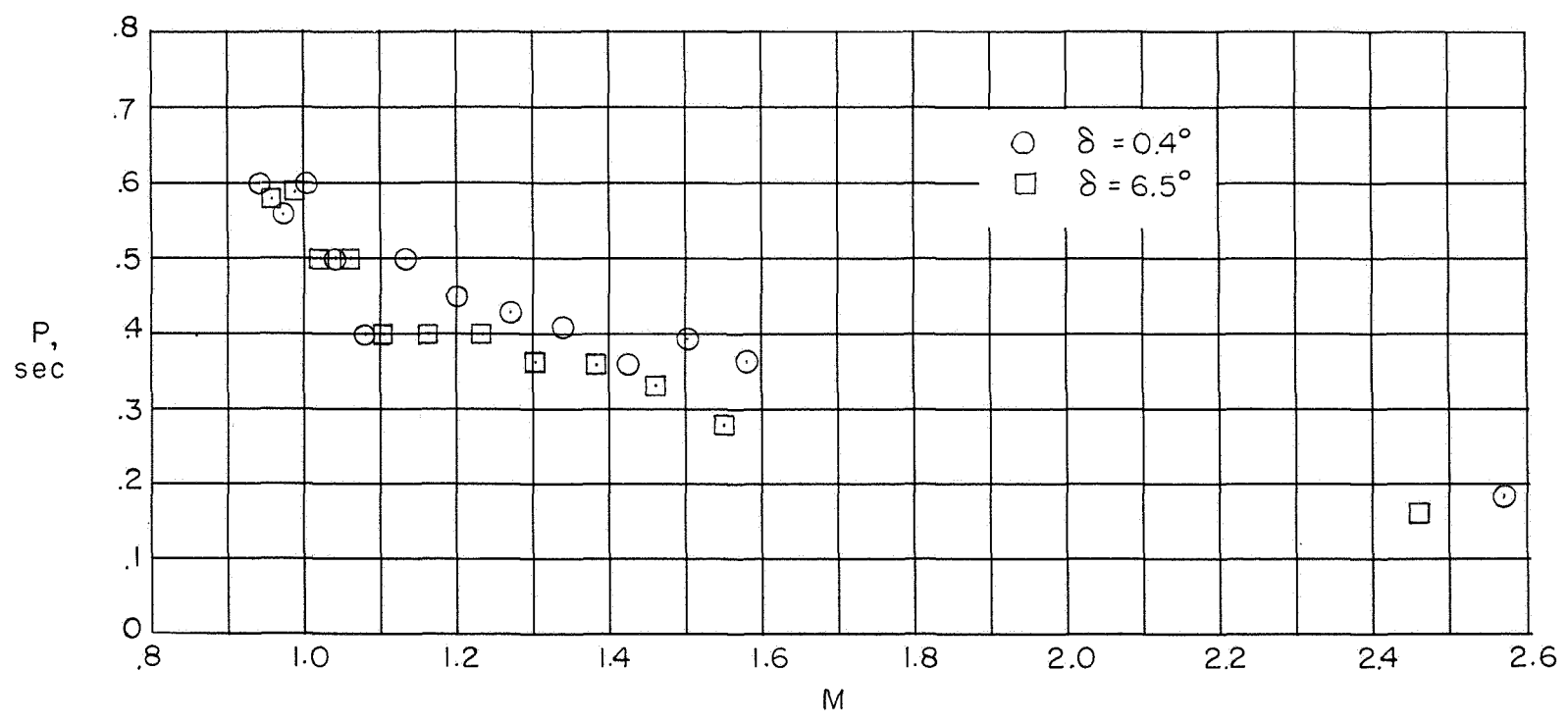


Figure 15.- Period of longitudinal oscillations.

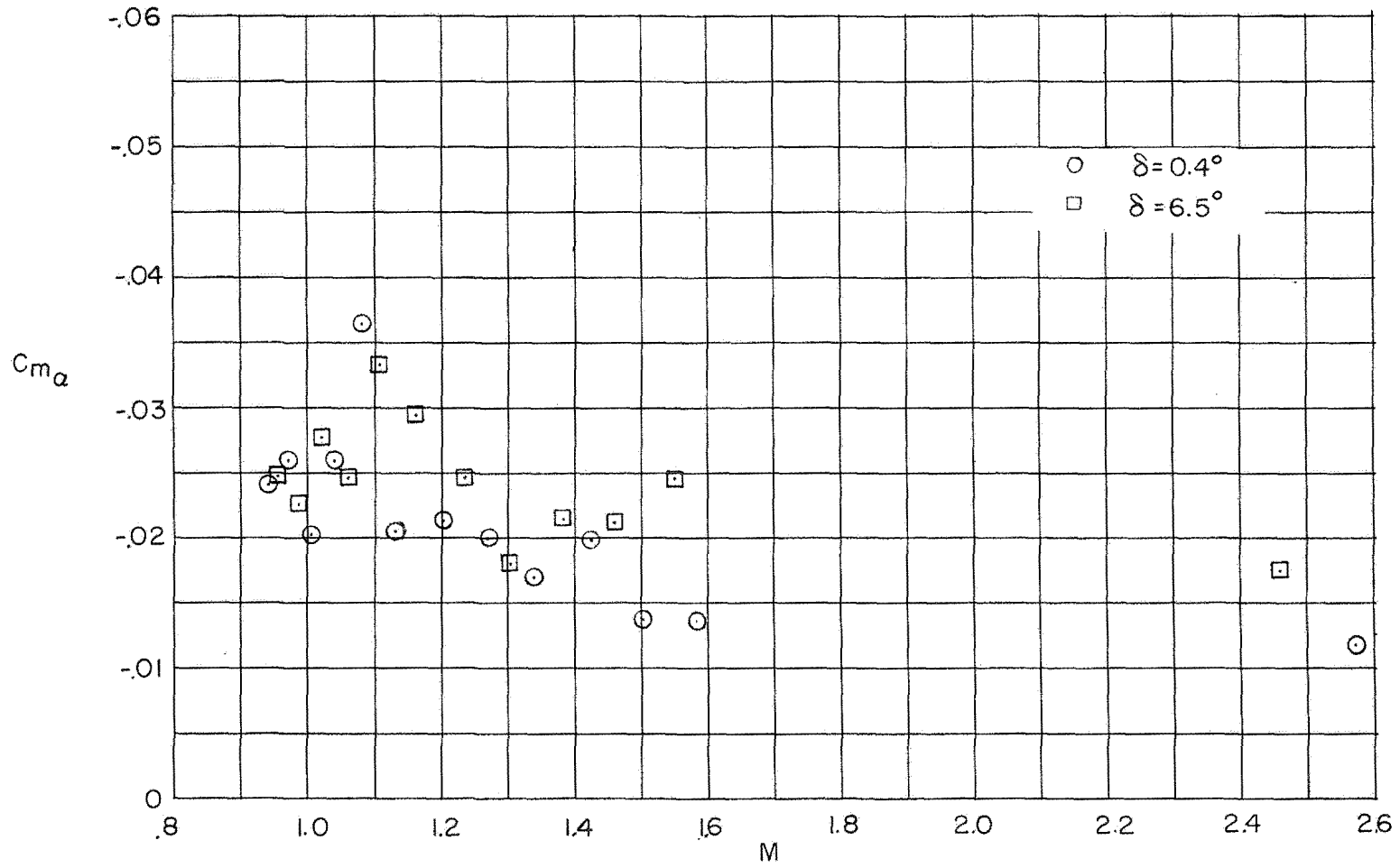
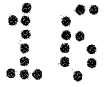
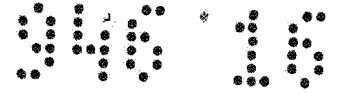
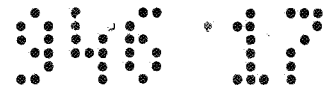


Figure 16.- Static stability derivative.



CONFIDENTIAL

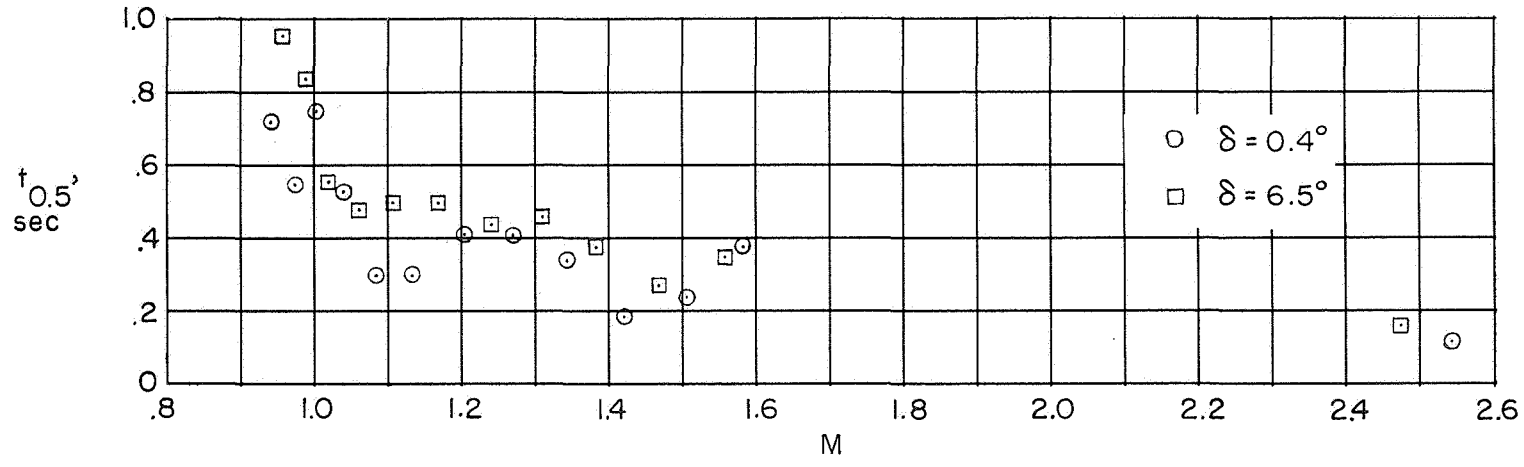


Figure 17.- Time to damp to one-half amplitude.

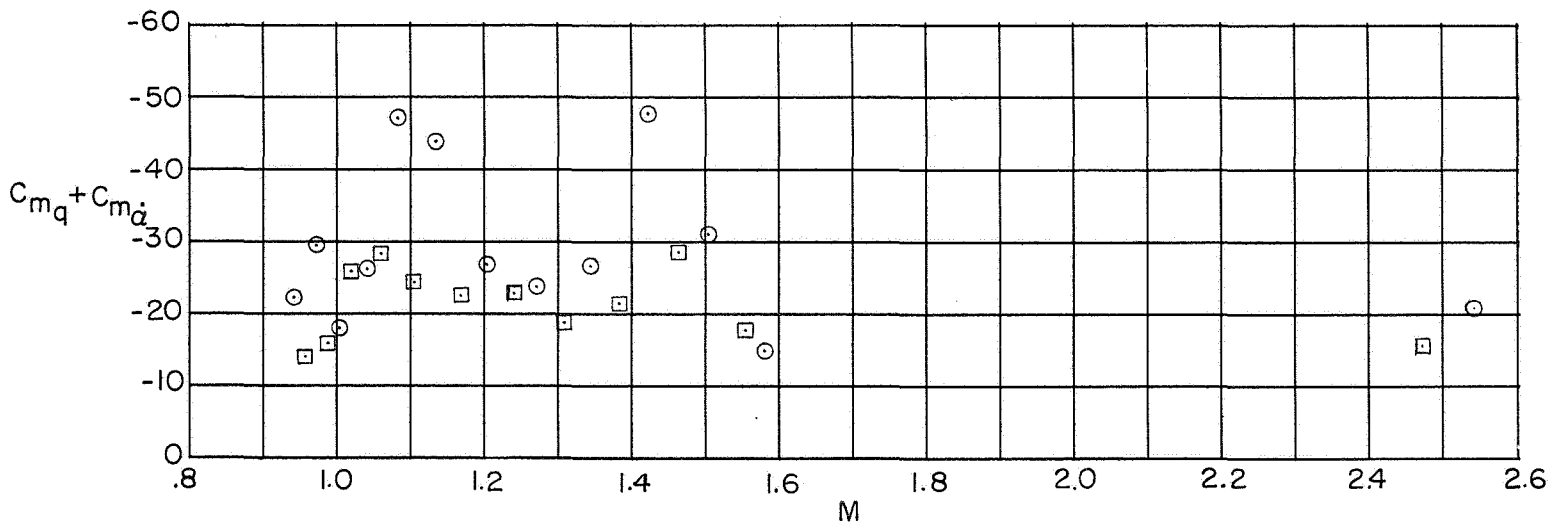


Figure 18.- Pitch damping derivative.

CONFIDENTIAL

CONFIDENTIAL

CONFIDENTIAL

CONFIDENTIAL





SERVICE REPORT

